

Downlink Power Optimization for Heterogeneous Networks with Time Reversal-based Transmission under Backhaul Limitation

Ha-Vu Tran¹, Georges Kaddoum¹, Hung Tran², and Een-Kee Hong³

Abstract—In this paper, we investigate an application of two different beamforming techniques and propose a novel downlink power minimization scheme for a two-tier heterogeneous network (HetNet) model. In this context, we employ time reversal (TR) technique to a femtocell base station (FBS) whereas we assume that a macrocell base station (MBS) uses a zero-forcing-based algorithm and the communication channels are subject to frequency selective fading. Additionally, HetNet's backhaul connection is unable to support a sufficient throughput for signaling information exchange between two tiers. Given the considered HetNet model, a downlink power minimization scheme is proposed, and closed-form expressions concerning the optimal solution are provided, taking this constraint into account. Furthermore, considering imperfect channel estimation at TR-employed femtocell, a worst-case robust power minimization problem is formulated. By devising TR worst-case analysis, this robust problem is transformed into an equivalent formulation that is tractable to solve. The results presented in our paper show that the TR technique outperforms the zero-forcing one in the perspective of beamforming methods for femtocell working environments. Finally, we validate the proposed power loading strategy for both cases of perfect and imperfect channel estimations.

Index Terms—Time reversal, heterogeneous networks, power allocation, beamforming, channel estimation error, frequency selective channel.

I. INTRODUCTION

Recently, heterogeneous network (HetNet) has been considered as a promising solution to enhance the throughput and to overcome the drawbacks of traditional cellular networks [1]–[3], such as the inefficient usage of spectrum and dynamic spectrum access. According to the HetNet concept, the macrocell serves a large number of users in a wide area while low power cells such as femtocells, picocells and microcells handle a smaller number of users. Following this approach, not only the coverage range is expanded but also the throughput and reliability can be improved significantly. More specifically, the works reported in [1]–[4] have investigated a HetNet model in which an original cellular network is decomposed into multi-tier networks, and each tier is responsible for a specific zone.

These approaches have expanded the coverage ranges over the dead zones and hot zones of traditional cellular networks. Therefore, the *femtocell* is considered as one of the most cost-efficient provisioning for cellular network services [5].

Regarding the radio environment, the signal power is often degraded due to path-loss effects and multipath propagation, and such an issue becomes more severe in the frequency selective fading. On the other hand, many techniques have been employed to mitigate the adverse effects of frequency selective channels such as: equalizers, multiple-input multiple-output (MIMO) and time reversal (TR) techniques. When applied to wireless receivers, the first two techniques provide significant enhancement to the received signal-to-noise ratio (SNR). However, from the implementation point of view, these techniques are high-cost and require complex equipment which make them less interesting to be used at the subscriber end where limited energy and processing resources are the major constraints.

However, a special class of beamforming technique, namely the TR, which was mainly used in acoustics and underwater communication systems, has been proposed in [6]–[13] to wireless communications, e.g. ultra-wideband, large-scale antenna, and millimeter-wave systems. This technique provides a promising solution to save the processing cost and to combat the adverse effects of frequency selective fading channels. Benefiting from the reciprocal properties of wireless channels, the TR technique principles rely on using the time-reversed form of a channel impulse response (CIR) to pre-filter the transmitted signal which leads to the power convergence of this latter in the time and space domains at the receiver side. Specifically, the CIR at the transmitter side is estimated by virtue of a pilot signal sent from the receiver.

Particularly, some works have addressed the designs of TR beamforming. In [8], the authors have provided an analysis of the TR technique for green radio communications employed to WiFi-certified technologies. The work [14] proposes three forms of space-time block diagonalization on the platform of the TR technique. Further, Yang *et al.* [15] propose a novel TR waveform to maximize the sum-rate of a multi-user system. In addition, the paper [16] introduces a design of a TR-based waveform using predistortion to combat inter-symbol interference (ISI). In fact, encouraging results obtained in [8]–[10] show that the TR-based transmission is an ideal paradigm for green wireless communications. Moreover, the experiments in [17], [18] confirm that the TR technique is feasible for broadband systems including femtocell networks.

¹Ha-Vu Tran and Georges Kaddoum are with University of Québec, ÉTS engineering school, LACIME Laboratory, 1100 Notre-Dame west, H3C 1K3, Montreal, Canada. Email: {ha-vu.tran.1@ens.etsmtl.ca, georges.kaddoum@etsmtl.ca.}

²Hung Tran is with School of Innovation, Design and Engineering, Mälardalen University, 721 23 Västerås, Sweden. Email: {tran.hung@mdh.se}

³Een-Kee Hong is with School of Electronics and Information, Kyung Hee University, Yongin 449-701, South Korea. Email: {ekhong@khu.ac.kr}

This work has been supported by NSERC discovery grant 435243 - 2013.

In our paper, we focus on studying a realistic scenario of HetNet system consisting of macrocell base station (MBS) and femtocell base station (FBS) and their users under backhaul limitation. The different channels in this network are subject to frequency selective fading. In our model, it is assumed that different cellular stations are equipped with multiple antennas whereas each receiver has one antenna due to the limited resources at the user end. Conventionally, a central controller, likely MBS, is responsible to compute the beamformers and power vectors for each base station (BS) located in the HetNet. Hence, this process requires a solid backhaul connections that must be always available to accommodate the central controller with all channel state information (CSI) of the different users located in different cells [4], [19]. However, in a realistic case that backhaul connection endures congestion in which obtaining sufficient amount of CSI might become infeasible. Therefore, given the system model, this work aims at seeking solutions for the question that *how to mitigate the frequency selectivity of fading channels, and to deal with the limited backhaul connection while taking the processing burden of the macrocell and the transmit power restriction of the femtocell network into account?* In the following, the potential proposed methods are discussed.

In this vein, one of our novelties consists of applying zero-forcing and TR techniques to MBS and FBS respectively to combat channel selectivity and to enhance network performance. In fact, zero-forcing is one of the most efficient beamforming techniques, and it is an interesting solution for macrocell networks [20], [21]. However, in a femtocell working environment where FBS's transmit power is limited, zero-forcing might not be a promising approach due to the transmit power restriction and hardware limitation [1], [20], [22]. In this case, the TR which offers an alternative low-cost beamforming technique, is proposed to provide a better system performance for femtocell networks.

Moreover, we propose a novel optimal power allocation method, assuming that the backhaul connection may only convey a limited throughput for signaling exchange. In single-tier multi-cell networks, the concept of cross-interference management has been introduced to deal with backhaul limitation [19]. However, this approach might not be applied to multi-tier HetNets directly since macrocell users (MUs) and femtocell users (FUs) have different priorities. Besides, there are several previous works addressing the issue of backhaul limitation for HetNets [23], [24]. In principle, these works focus on splitting the conventional optimization problem into two subproblems (i.e. one for the macrocell and the other for the femtocell) in which solutions can be achieved with a reduced amount of required CSI. In our work, decoupling the original problem is adopted in a different manner to deal with backhaul limitation. In particular, the proposed scheme only requires the minimized cross-tier interference sent from the femtocell. This latter reduces the signaling overhead in the network compared with the scheme proposed in [23], and releasing the FUs from the task of measuring cross-interference caused by the MBS compared with the another work [24]. Moreover, importantly, our scheme can control the priority of MUs by using a preset threshold of the cross-tier interference that the MBS causes

to the FUs. On this basis, the network operator can flexibly manage the overall network performance. Especially, we solve the considered macrocell and femtocell problems by devising optimal closed-form solutions which do not appear in the literature.

Furthermore, most of previous publications [8], [9], [14], [16] address the designs of TR beamforming under the assumption of perfect channel estimations. There are no existing works which consider the worst-case robust beamforming for the TR technique. Given this concern, the robust design is formulated into a non-convex problem. To transform such a problem into a tractable formulation to solve, the effects of channel estimation errors (CEE) on TR-based systems are analyzed in terms of the worst-case boundaries of desired signal and interference components. Especially, to tackle this case, a well-known Young's inequality [25] is able to bring an efficient solution dealing with the boundaries of ISI and co-tier interference. However, a novel tighter boundary formulation is derived to enhance the performance of power allocation strategy. On this basis, the robust optimization problem is relaxed into a convex problem that can be solved by closed-form expressions.

According to the discussed content, the main contributions of this work are summarized as follows

- The application of TR technique for the femtocell network is proposed.
- A novel downlink optimization method dealing with limited backhaul connections is provided.
- Closed-form optimal solutions are derived for both the downlink power minimization problems of macrocell and femtocell.
- A robust worst-case power allocation problem of TR-employed femtocell under the effects of imperfect CSI is analyzed.

Given this outline, the remainder of this paper is organized as follows: In Section II, the system model is described. The beamforming designs for MBS and FBS are discussed in Section III. In Section IV, the proposed power allocation manner is presented. In Section V, the worst-case robust problem is formulated and analyzed. In Section VI, numerical results and discussions are provided. Finally, concluding remarks are put forward in Section VII.

Notation: The notation \mathbb{R}_+^m and $\mathbb{C}^{m \times n}$ denote the sets of m -dimensional nonnegative real vector and $m \times n$ complex matrix, respectively. The boldface lowercase \mathbf{a} and uppercase \mathbf{A} indicate vectors and matrices, respectively. The superscripts \mathbf{A}^T and \mathbf{A}^H represent the transpose and transpose conjugate, respectively. In addition, symbols $|\cdot|$, $\|\cdot\|$, and $\|\cdot\|_1$ stand for the absolute value, vector Euclidean norm and vector l_1 -norm, respectively. For a complex value, we denote $\Re\{\cdot\}$ and $\Im\{\cdot\}$ to be the real and imaginary part, respectively.

II. SYSTEM MODEL

As shown in Fig. 1, a two-tier HetNet system including one MBS and one FBS is considered. For convenient notation, we denote the MBS as \mathcal{B}_0 and the FBS as \mathcal{B}_1 . We assume that \mathcal{B}_k ($k = \{0, 1\}$) is equipped with M_k antennas and serves N_k

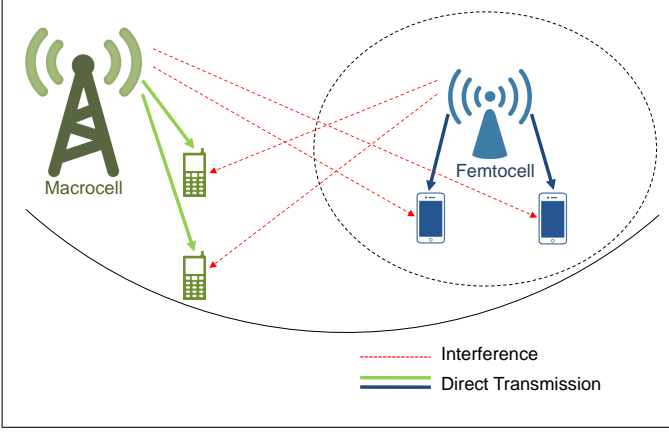


Fig. 1. A two-tier system model including a macrocell and a femtocell.

users. On the other hand, FUs and MUs are equipped with a single antenna and a single tap diversity combiner.

Let $\mathbf{h}_{ij}^{kr} \in \mathbb{C}^{L \times 1}$ ($k, r = \{0, 1\}$, $0 \leq i \leq M_k$, $0 \leq j \leq N_r$) denote the CIR between the i^{th} transmission antenna of \mathcal{B}_k and the j^{th} user of \mathcal{B}_r . Moreover, L denotes the maximum length of each CIR, and the superscript k is used to represent superscript kk for convenience in notation, (e.g. \mathbf{h}_j^0 is used to denote \mathbf{h}_j^{00}).

Therefore, the transmitted signals at \mathcal{B}_0 and \mathcal{B}_1 can be formulated, respectively, as

$$\mathbf{x}_n^0 = \sqrt{p_n^0} [\mathbf{u}_{1n} \ \dots \ \mathbf{u}_{M_0n}] s_n^0, (\mathbf{x}_n^0 \in \mathbb{C}^{L \times M_0}) \quad (1)$$

$$\mathbf{x}_j^1 = \sqrt{p_j^1} [\mathbf{g}_{1j} \ \dots \ \mathbf{g}_{M_1j}] s_j^1, (\mathbf{x}_j^1 \in \mathbb{C}^{L \times M_1}) \quad (2)$$

where s_n^0 and s_j^1 are scalars representing the unit power transmitted symbols for the n^{th} MU and the j^{th} FU, respectively. We define $\mathbf{p}^k = [p_1^k \ p_2^k \ \dots \ p_{N_k}^k]^T \in \mathbb{R}_+^{N_k \times 1}$ as the transmit power vector of the \mathcal{B}_k . Furthermore, $\mathbf{u}_{mn} \in \mathbb{C}^{L \times 1}$ is the beamformer for the n^{th} MU used at the m^{th} transmission antenna, and $\mathbf{g}_{ij} \in \mathbb{C}^{L \times 1}$ is the beamformer for the j^{th} FU employed at the i^{th} transmit antenna. Specifically, \mathbf{u}_{mn} follows a zero-forcing-based algorithm whereas \mathbf{g}_{ij} has the formulation of TR beamformer. The design of two such beamforming vectors is thoroughly discussed in Section IV. A and Section IV. B.

In our paper, we consider the downlink communication scenario in which the MBS and the FBS transmit their signals to their corresponding users simultaneously and none of these communicate with its BS during this phase of communication. Accordingly, the received signal at the n^{th} MU can be written as

$$\begin{aligned} \mathbf{y}_n^0 &= \sum_{m=1}^{M_0} \sqrt{p_n^0} \mathbf{u}_{mn} * \mathbf{h}_{mn}^0 s_n^0 + \sum_{\substack{n'=1 \\ n' \neq n}}^{N_0} \sum_{m=1}^{M_0} \sqrt{p_{n'}^0} \mathbf{u}_{mn'} * \mathbf{h}_{mn}^0 s_{n'}^0 \\ &+ \sum_{j=1}^{N_1} \sum_{i=1}^{M_1} \sqrt{p_j^1} \mathbf{g}_{ij} * \mathbf{h}_{in}^{10} s_j^1 + \mathbf{n}_M, (\mathbf{y}_n^0 \in \mathbb{C}^{(2L-1) \times 1}) \end{aligned} \quad (3)$$

where \mathbf{n}_M is additive white Gaussian noise (AWGN), and $*$ is the convolution operator. It is noted that the first term in (3) is the received signal of the n^{th} MU while the second term is

the co-tier interference in the macrocell and the third term is the cross-tier interference from the femtocell.

Hence, at the n^{th} MU, we define $P_{(sig)_n}^0$, $P_{(isi)_n}^0$, $P_{(co)_n}^0$, and $P_{(cross)_n}^0$ as the power of desired signal, ISI, co-tier interference power and cross-tier interference from femtocell, respectively, as indicated in (4)-(7).

$$P_{(sig)_n}^0 = \left| \left(\sum_{m=1}^{M_0} \sqrt{p_n^0} \mathbf{u}_{mn} * \mathbf{h}_{mn}^0 \right) [\alpha] \right|^2, \quad (4)$$

$$P_{(isi)_n}^0 = \sum_{l \neq \alpha}^{2L-1} \left| \left(\sum_{m=1}^{M_0} \sqrt{p_n^0} \mathbf{u}_{mn} * \mathbf{h}_{mn}^0 \right) [l] \right|^2, \quad (5)$$

$$P_{(co)_n}^0 = \sum_{\substack{n'=1 \\ n' \neq n}}^{N_0} \left\| \sum_{m=1}^{M_0} \sqrt{p_{n'}^0} \mathbf{u}_{mn'} * \mathbf{h}_{mn}^0 \right\|^2, \quad (6)$$

$$P_{(cross)_n}^0 = \sum_{j=1}^{N_1} \left\| \sum_{i=1}^{M_1} \sqrt{p_j^1} \mathbf{g}_{ij} * \mathbf{h}_{in}^{10} \right\|^2, \quad (7)$$

where α represents the position of the selected tap.

Accordingly, the signal-to-interference-plus-noise ratio (SINR) at the n^{th} MU can be formulated as

$$\begin{aligned} \text{SINR}_n^0 &= \frac{P_{(sig)_n}^0}{P_{(isi)_n}^0 + P_{(co)_n}^0 + P_{(cross)_n}^0 + \|\mathbf{n}_M[\alpha]\|^2}, \end{aligned} \quad (8)$$

On the other hand, the received signal at the j^{th} FU can be expressed as

$$\begin{aligned} \mathbf{y}_j^1 &= \sum_{i=1}^{M_1} \sqrt{p_j^1} \mathbf{g}_{ij} * \mathbf{h}_{ij}^1 s_j^1 + \sum_{\substack{j'=1 \\ j' \neq j}}^{N_1} \sum_{i=1}^{M_1} \sqrt{p_{j'}^1} \mathbf{g}_{ij'} * \mathbf{h}_{ij}^1 s_{j'}^1 \\ &+ \sum_{n=1}^{N_0} \sum_{m=1}^{M_0} \sqrt{p_n^0} \mathbf{u}_{mn} * \mathbf{h}_{mj}^{01} s_n^0 + \mathbf{n}_F, (\mathbf{y}_j^1 \in \mathbb{C}^{(2L-1) \times 1}) \end{aligned} \quad (9)$$

where \mathbf{n}_F is AWGN. Here, the first term in (9) is the received signal for the j^{th} FU, the second term is the co-tier interference in the femtocell, and the third term is the cross-tier interference from the macrocell.

Similarly, $P_{(sig)_j}^1$, $P_{(isi)_j}^1$, $P_{(co)_j}^1$, and $P_{(cross)_j}^1$, i.e. (10)-(13), represent the power of the desired signal, ISI, co-tier interference and cross-tier interference from macrocell, respectively.

$$P_{(sig)_j}^1 = \left| \left(\sum_{i=1}^{M_1} \sqrt{p_j^1} \mathbf{g}_{ij} * \mathbf{h}_{ij}^1 \right) [\beta] \right|^2, \quad (10)$$

$$P_{(isi)_j}^1 = \sum_{\substack{l=1 \\ l \neq \beta}}^{2L-1} \left| \left(\sum_{i=1}^{M_1} \sqrt{p_j^1} \mathbf{g}_{ij} * \mathbf{h}_{ij}^1 \right) [l] \right|^2, \quad (11)$$

$$P_{(co)}^1_j = \sum_{\substack{j'=1 \\ j' \neq j}}^{N_1} \left\| \sum_{i=1}^{M_1} \sqrt{p_{j'}^1} \mathbf{g}_{ij'} * \mathbf{h}_{ij}^1 \right\|^2, \quad (12)$$

$$P_{(cross)}^1_j = \sum_{n=1}^{N_0} \left\| \sum_{m=1}^{M_0} \sqrt{p_n^0} \mathbf{u}_{mn} * \mathbf{h}_{mj}^{01} \right\|^2, \quad (13)$$

where β denotes the position of selected tap. Note that the problem of selecting the values of α and β is discussed in the following Section IV.

Thus, the SINR of the j^{th} FU can be expressed as

$$\begin{aligned} \text{SINR}_j^1 & \left(\beta, \mathbf{p}^1, \{\mathbf{g}_{ij}^1\}_{i=1, j=1}^{M_1, N_1}, P_{(cross)}^1_j \right) \\ &= \frac{P_{(sig)}^1_j}{P_{(isi)}^1_j + P_{(co)}^1_j + P_{(cross)}^1_j + \|\mathbf{n}_F[\beta]\|^2}. \end{aligned} \quad (14)$$

III. BEAMFORMING DESIGNS FOR THE MBS AND THE FBS

This section provides the beamforming designs for FBS and MBS over frequency selective fading channels. In more details, MBS uses a zero-forcing-based algorithm whereas FBS employs the TR technique.

A. Beamformer design following the zero-forcing technique for the MBS

It is well-known that the zero-forcing technique mainly aims to suppress the interference components. Also, such a technique leads to the fact that the desired signal strength might only reach a limited level. However, this issue can be overcome by using a high transmit power. Given this concern, the signal strength can be significantly improved whereas the interference is cancelled. Due to the availability of power at MBS, zero-forcing beamforming technique is preferred as an efficient solution in such an environment. On the other hand, user receivers take only one sample at a particular tap. For the l^{th} case, we specifically treat the l^{th} tap as the desired tap whereas the other taps can be considered as the ISI taps respectively. The corresponding beamformer must be designed following the zero-forcing scheme to suppress both ISI and co-tier interference. Thereupon, we obtain $(2L-1)$ relevant beamformers. Finally, we finger out the beamformer among these candidates that yields the best SINR at the user. In the following content, the zero-forcing-based algorithm is discussed in details.

Let us start with a beamforming design based on the well-known zero-forcing technique over macrocell environments by re-arranging values of $\{\mathbf{h}_{mn}^0[l]\}_{m=1}^{M_0}$ into a new form $\bar{\mathbf{h}}_{ln} \in \mathbb{C}^{1 \times M_0}$ as follows

$$\bar{\mathbf{h}}_{ln} = [h_{1n}^0[l] \ h_{2n}^0[l] \ \dots \ h_{M_0n}^0[l]]. \quad (15)$$

Further, we define a matrix $\bar{\mathbf{H}}_n \in \mathbb{C}^{(2L-1) \times M_0L}$ as

$$\bar{\mathbf{H}}_n = \begin{bmatrix} \bar{\mathbf{h}}_{1n} & \mathbf{0} & \mathbf{0} \\ \bar{\mathbf{h}}_{2n} & \bar{\mathbf{h}}_{1n} & \mathbf{0} \\ \vdots & \bar{\mathbf{h}}_{2n} & \mathbf{0} \\ \bar{\mathbf{h}}_{Ln} & \vdots & \ddots & \bar{\mathbf{h}}_{1n} \\ & \bar{\mathbf{h}}_{Ln} & & \bar{\mathbf{h}}_{2n} \\ & & \ddots & \vdots \\ \mathbf{0} & & & \bar{\mathbf{h}}_{Ln} \end{bmatrix}. \quad (16)$$

Note that the matrix $\bar{\mathbf{H}}_n$ is derived following the formulation of the Sylvester matrix of $(\mathbf{h}_{mn}^0)^T$ [pp. 28, [26]]. For each sampled tap $\bar{\alpha}^{\text{th}}$, let us define $\bar{\mathbf{u}}_{mn, \bar{\alpha}} \in \mathbb{C}^{L \times 1}$ as the $\bar{\alpha}^{\text{th}}$ candidate for the beamformer \mathbf{u}_{mn} .

On the basis of zero-forcing principle, the beamformer of MBS can be derived according to a computation as follows

$$\text{vec}([\bar{\mathbf{u}}_{1n, \bar{\alpha}} \ \bar{\mathbf{u}}_{2n, \bar{\alpha}} \ \dots \ \bar{\mathbf{u}}_{M_0n, \bar{\alpha}}]) = c_{n, \bar{\alpha}} \bar{\mathbf{H}}_n^\dagger \mathbf{z}_{n, \bar{\alpha}}, \quad (17)$$

where $\bar{\mathbf{H}} = [\bar{\mathbf{H}}_1^T \ \bar{\mathbf{H}}_2^T \ \dots \ \bar{\mathbf{H}}_{N_0}^T]^T$, $c_{n, \bar{\alpha}}$ is a normalization factor, $\mathbf{z}_{n, \bar{\alpha}} = [\mathbf{0}^T \ \dots \ \mathbf{0}^T \ \mathbf{s}_{\bar{\alpha}} \ \mathbf{0}^T \ \dots \ \mathbf{0}^T]^T$, in which $\mathbf{s}_{\bar{\alpha}}$ is the n -th vector of $\mathbf{z}_{n, \bar{\alpha}}$ and $\mathbf{s}_{\bar{\alpha}} = [0 \ \dots \ 0 \ 1 \ 0 \ \dots \ 0]^T \in \mathbb{R}_+^{(2L-1) \times 1}$ (the 1 is located at the $\bar{\alpha}^{\text{th}}$ index), and $(\cdot)^\dagger$ denotes Moore-Penrose pseudo-inverse operator.

Thus, the $\bar{\alpha}^{\text{th}}$ candidate for the beamformer component given in (1) can be represented as

$$[\bar{\mathbf{u}}_{1n, \bar{\alpha}} \ \bar{\mathbf{u}}_{2n, \bar{\alpha}} \ \dots \ \bar{\mathbf{u}}_{M_0n, \bar{\alpha}}] = \text{vec}^{-1}(c_{n, \bar{\alpha}} \bar{\mathbf{H}}_n^\dagger \mathbf{z}_{n, \bar{\alpha}}), \quad (18)$$

Specifically, in the case that the matrix $\bar{\mathbf{H}}$ has a right-inverse, the interference components are completely cancelled. Hence, the received signal at n^{th} MU can be simplified as

$$\mathbf{y}_n^0 = \sqrt{p_n^0} c_{n, \bar{\alpha}} \mathbf{s}_{\bar{\alpha}} s_n^0 + \sum_{j=1}^{N_1} \sum_{i=1}^{M_1} \sqrt{p_j^1} \mathbf{g}_{ij} * \mathbf{h}_{in}^{10} s_j^1 + \mathbf{n}_M, \quad (19)$$

On the other hand, for mathematical simplification, we define a factor $\Gamma_{n, \bar{\alpha}}$ shown in (20). This factor is to evaluate the ratio between the power of the main tap and that of the interferences. To this end, we present the details of the beamforming design in *Algorithm 1* for a comprehensive idea.

Algorithm 1: Algorithm to solve \mathbf{u}_{mn}

(i). Set $\bar{\alpha} = 1$.

(ii). **Loop**

1. Compute $\bar{\mathbf{u}}_{mn, \bar{\alpha}}$ by (17).

2. Calculate $\Gamma_{n, \bar{\alpha}}$ by (20).

3. Update $\bar{\alpha} \leftarrow \bar{\alpha} + 1$.

Until $\bar{\alpha} = 2L - 1$.

(iii). Find α with

$$\alpha = \arg \max_{\bar{\alpha}} \{\{\Gamma_{n, \bar{\alpha}}\}_{\bar{\alpha}=1}^{2L-1}\}.$$

(iv). The chosen beamformer \mathbf{u}_{mn} can be inferred from $\bar{\mathbf{u}}_{mn, \alpha}$.

$$\Gamma_{n,\bar{\alpha}} = \frac{\left| \left(\sum_{m=1}^{M_0} \bar{\mathbf{u}}_{mn,\bar{\alpha}} * \mathbf{h}_{mn}^0 \right) [\bar{\alpha}] \right|^2}{\sum_{l \neq \bar{\alpha}}^{2L-1} \left| \left(\sum_{m=1}^{M_0} \bar{\mathbf{u}}_{mn,\bar{\alpha}} * \mathbf{h}_{mn}^0 \right) [l] \right|^2 + \sum_{n' \neq n}^{N_0} \sum_{l=1}^{2L-1} \left| \left(\sum_{m=1}^{M_0} \bar{\mathbf{u}}_{mn',\bar{\alpha}} * \mathbf{h}_{mn'}^0 \right) [l] \right|^2 + 1}. \quad (20)$$

B. Time Reversal beamforming technique for the FBS

Unlike MBS, FBS is a low-power cellular station with limited hardware resources [1], [4]. This limitation is due to the fact that the zero-forcing beamformer includes the component of matrix inversion, with a huge computational burden that becomes extremely heavy in cases of many users and lengthy CIRs. Furthermore, the transmit power level of FBS is restricted [1]. Therefore, the zero-forcing technique might not be an interesting solution for femtocell networks.

In this paper, we propose employing the TR technique to FBS to achieve a better system performance with a much reduced cost. Indeed, the location signature-specific property of the TR can be utilized to mitigate the ISI, the co-tier interference and the cross-tier interference to the macrocell [8], [16].

According to (2), the FBS beamformer can be expressed by

$$\begin{bmatrix} \mathbf{g}_{1j} & \dots & \mathbf{g}_{M_{1j}} \end{bmatrix} = \begin{bmatrix} g_{1j}[1] & \dots & g_{M_{0j}}[1] \\ g_{1j}[2] & \dots & g_{M_{0j}}[2] \\ \vdots & \vdots & \vdots \\ g_{1j}[L] & \dots & g_{M_{0j}}[L] \end{bmatrix}. \quad (21)$$

In TR principle, the time-reversed form of CIR is employed as FBS beamformer, thus each element of \mathbf{g}_{ij} can be calculated as

$$g_{ij}[l] = \frac{h_{ij}^{1H}[L+1-l]}{\sqrt{\sum_{i=1}^{M_1} \|\mathbf{h}_{ij}^1\|^2}}. \quad (22)$$

Benefiting from the signal focalization property of the TR technique, FU receivers need only to select the central tap to take a sample, i.e. $\beta = L$. As one can evaluate, the TR technique has a much lower computational complexity in comparison to the zero-forcing one.

IV. PROPOSED POWER ALLOCATION APPROACH

In this section, we propose a novel downlink power allocation scheme for the considered HetNet taking into account the fact that the backhaul connection is unable to convey all user CSI from femtocell to macrocell. We start with briefly presenting the centralized power allocation approach in order to understand this concept and compare its performance to the proposed approach. In the centralized method, a central controller, likely MBS, is responsible of computing the beamforming and power allocation vectors for all BSs in the HetNet. Assuming that all the CSI of MUs and FUs are available at the MBS, the power control problem which minimizes the

total transmit power of BSs with SINR constraints can be formulated as

$$\begin{aligned} \text{OP}_0 : \min_{\mathbf{p}^0, \mathbf{p}^1} & \sum_{k=0}^1 \sum_{r=1}^{N_k} p_r^k \\ \text{s.t.} & \text{SINR}_r^k \geq \gamma_r^k, (\forall k \in \{0, 1\}; 1 \leq r \leq N_k), \end{aligned} \quad (23)$$

herein γ_r^k is the preset threshold for the r^{th} user of \mathcal{B}_k . Since we divide the downlink power allocation and the beamforming procedures into distinct processes, the optimization problem in (23) becomes convex on \mathbf{p}^k and the optimal solution can be conveniently found [27], [28].

Given this centralized approach, the femtocell needs to send all FU CSI to the macrocell via the backhaul link. Therefore, signaling overheads as well as computational burdens at the macrocell are heavy when the network size is large. However, in case of link congestion, obtaining sufficient CIR becomes intractable. Due to these drawbacks, a novel scheme is proposed for the considered HetNet. In this vein, the original optimization problem OP_0 given in equation (23) is decomposed into two subproblems, i.e. MBS subproblem and FBS subproblem, to (i) share computational burden to all BSs and (ii) reduce the dependence on backhaul links. Different from previous works [19], [23], [24], our proposed optimization method can perform as follows: (i) To reduce the amount of signaling information, the FBS computes first the beamforming vector for its own users, then optimizes the corresponding transmission power to mitigate the cross-tier interference to the MUs and finally transfers the minimized value of the cross-tier interference power to the MBS. (ii) Afterwards, the MBS initiates computing its own beamformer and power allocation vector once it receives the specific information sent by the FBS. Hence, this method limits the signaling overhead since only a minimized value of the cross-tier interference power is required at the MBS side. In addition, the FUs are released from the task of measuring the cross-interference caused by the MBS. Importantly, our scheme can allow the operator to control the priority of MUs, shown in subsection IV.A. Furthermore, the optimal closed-form solutions are derived for such subproblems. A comparison between two the centralized and proposed approaches is shown in Fig. 2. In this regard, the required amount of signaling exchange between two tiers becomes much smaller (i.e. Table I), and the proposed scheme can achieve near optimal performance. To this end, the subproblems for femtocell and macrocell are thoroughly discussed in the following subsections.

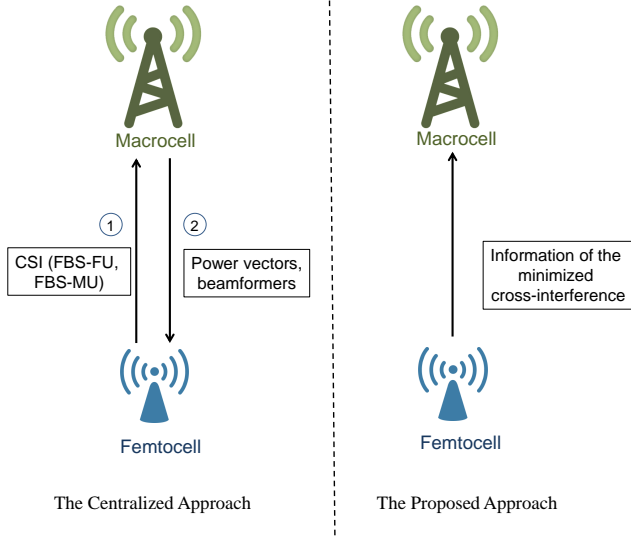


Fig. 2. A comparison between the approaches.

TABLE I
THE CSI REQUIRED AT MBS

Kinds of CSI	Centralized approach	Proposed approach
MBS - MU	required	required
MBS - FU	required	required
FBS - MU	required	not required
FBS - FU	required	not required

A. Subproblem 1: Power allocation for the FBS

In HetNet, both MUs and FUs frequently endure the cross-tier interference, but MUs have a higher priority than FUs in communication such that optimization designs must satisfy MUs quality of service (QoS). Therefore, to give priority to MUs, the femtocell should minimize the interference that it causes to MUs. On the other hand, to reduce the CSI sent to MBS, the femtocell starts the communication by providing an optimized power allocation with respect to a tolerable level of cross-tier interference that is set for each FU as $P_{(tol)j}^{01}$. Accordingly, the downlink power control problem for the FBS can be interpreted as

$$\begin{aligned}
 \text{OP}_1: \min_{\mathbf{p}^1} & \sum_{j=1}^{N_1} \left(\sum_{n=1}^{N_0} \left\| \sum_{i=1}^{M_1} \mathbf{g}_{ij} * \mathbf{h}_{in}^{10} \right\|^2 p_j^1 \right) \\
 \text{s.t.} & \text{SINR}_j^1 \left(L, \mathbf{p}^1, \{\mathbf{g}_{ij}\}_{i=1, j=1}^{M_1, N_1}, P_{(tol)j}^{01} \right) \geq \gamma_j^1. \\
 & (1 \leq j \leq N_1)
 \end{aligned} \quad (24)$$

Hence, the tolerable cross-tier interference implies that

$$P_{(cross)j}^1 = \sum_{n=1}^{N_0} \left\| \sum_{m=1}^{M_0} \sqrt{p_n^0} \mathbf{u}_{mn} * \mathbf{h}_{mj}^{01} \right\|^2 \leq P_{(tol)j}^{01}. \quad (25)$$

Moreover, the inequality given in (25) is set as a constraint of the MBS's power allocation problem, i.e. see (34).

In fact, although MUs are primary users, there should be restrictions applied in the cross-interference that MBS cause to FUs due to flexible management for operators. Given this

scheme, the operator might manage the priority level of MUs by adjusting the tolerable threshold, i.e. $\{P_{(tol)j}^{01}\}$. This makes the proposed scheme more flexible than the previous works [23], [24].

It is easy to see that the considered optimization problem requires the CSI at femtocells only, and the objective function aims to minimize the cross interference to MUs, i.e. $P_{(cross)n}^0$. On the other hand, it is visible that the problem OP_1 is a linear programming problem. Thus, the solution of problem OP_1 is summarized in Lemma 1 below.

Lemma 1. Let \mathbf{p}^{*1} denote the optimal value of \mathbf{p}^1 . Based on preliminaries in [18.4 [27]], [eq. (4) [28]], the closed-form expression of \mathbf{p}^{*1} can be given by

$$\mathbf{p}^{*1} = \text{diag}(\boldsymbol{\eta})^{-1} [\mathbf{I}_{N_1} - \text{diag}(\boldsymbol{\eta})\mathbf{D} (\mathbf{B} \circ (\boldsymbol{\eta}^{-1} \mathbf{1}_{N_1 \times 1}^T))]^{-1} \mathbf{z}, \quad (26)$$

where \circ denotes Hadamard product, \mathbf{I}_{N_1} is an $N_1 \times N_1$ identity matrix, \mathbf{B} is a $N_1 \times N_1$ matrix whose the (j, j') th entry is defined as

$$(\mathbf{B})_{j'j} = \begin{cases} 0, & j = j' \\ \left\| \sum_{i=1}^{M_1} \mathbf{g}_{ij'} * \mathbf{h}_{ij}^1 \right\|^2, & j \neq j', \end{cases} \quad (27)$$

in addition,

$$\boldsymbol{\eta} = \frac{\hat{\boldsymbol{\eta}}}{\|\hat{\boldsymbol{\eta}}\|}, \quad (28)$$

in which each element of the vector $\hat{\boldsymbol{\eta}} \in \mathbb{C}^{N_1}$ is

$$\hat{\eta}_j = \sum_{n=1}^{N_0} \left\| \sum_{i=1}^{M_k} \mathbf{g}_{ij} * \mathbf{h}_{in}^{10} \right\|^2, \quad (29)$$

and \mathbf{D} is a $N_1 \times N_1$ matrix which is presented by

$$\mathbf{D} = \text{diag} \left\{ \frac{\gamma_1^1}{\varphi_1}; \dots; \frac{\gamma_{N_1}^1}{\varphi_{N_1}} \right\}, \quad (30)$$

where

$$\varphi_j = \left| \left(\sum_{i=1}^{M_1} \mathbf{g}_{ij} * \mathbf{h}_{ij}^1 \right) [L] \right|^2 - \gamma_j^1 \sum_{\substack{l=1 \\ l \neq L}}^{2L-1} \left| \left(\sum_{i=1}^{M_1} \mathbf{g}_{ij} * \mathbf{h}_{ij}^1 \right) [l] \right|^2, \quad (31)$$

and \mathbf{z} is a vector $\mathbf{z} = [z_1 \ z_2 \ \dots \ z_{N_1}]^T$ with each element given as

$$z_j = P_{(tol)j}^{01} + \|\mathbf{n}_F[L]\|^2. \quad (32)$$

Proof: See Appendix A. ■

In the proposed scheme, when the femtocell tackles the optimization problem OP_1 , the value of $\{P_{(cross)n}^0\}_{n=1}^{N_0}$ given in equation (33) is sent to the macrocell instead of the information of \mathbf{p}^{*1} , $\{\mathbf{h}_{ij}^1\}_{i=1, j=1}^{M_1, N_1}$ and $\{\mathbf{h}_{in}^{10}\}_{j=1, n=1}^{N_1, N_0}$ via the backhaul link.

$$P_{(cross)n}^{*0} = \sum_{j=1}^{N_1} \left\| \sum_{i=1}^{M_1} \sqrt{p_j^{*1}} \mathbf{g}_{ij} * \mathbf{h}_{in}^{10} \right\|^2. \quad (33)$$

It is worth reminding that \mathbf{h}_{in}^{10} denotes the CIR between the femtocell and the n^{th} macrocell user. In other words, \mathbf{h}_{in}^{10} is the local CSI of the femtocell network. In our paper, \mathbf{h}_{in}^{10} is assumed to be available at the femtocell in both the centralized and the proposed approaches.

Therefore, in the proposed power allocation, one can conclude that the amount of overhead used for signaling information is significantly reduced.

B. Subproblem 2: Power loading problem for the MBS

In this part, we present our derivation methodology of the downlink power allocation for MBS. Our aim is to minimize the total transmit power with the interference constraint to FUs. To actively guarantee the performance for MUs, the MBS computes the beamforming and power allocation vectors once it receives the signaling information of $\{P_{(cross)n}^*\}_{n=1}^{N_0}$ given by (33) from the femtocell. Hence, the optimization problem involving the SINR and interference constraints is formulated as

$$\begin{aligned} \text{OP}_2: \min_{\mathbf{p}^0} \quad & \sum_{n=1}^{N_0} p_n^0 \\ \text{s.t.} \quad & \text{SINR}_n^0(\alpha, \mathbf{p}^0, \{\mathbf{u}_{mn}\}_{m=1, n=1}^{M_0, N_0}, P_{(cross)n}^*) \geq \gamma_n^0. \\ & \left\| \sum_{m=1}^{M_0} \sqrt{p_n^0} \mathbf{u}_{mn} * \mathbf{h}_{mj}^{01} \right\|^2 \leq P_{(tol)j}^{01}, \end{aligned} \quad (34)$$

The above problem is a linear programming problem which can be solved by interior-point method. To reduce the computational burden, we aim at solving OP_2 by closed-form expressions. Since the objective function and the constraints of OP_2 are not differentiable, it is infeasible to solve OP_2 through its the Lagrangian dual. To deal with this issue, we endeavour to transform the problem OP_2 into an equivalent formulation solvable by the Lagrange multiplier method.

In this context, we start with applying the uplink-downlink duality property to the SINR_n^0 constraint of the OP_2 . It is observed that the SINR_n^0 constraint can be considered as a function of $P_{(co)n}^0$. According to the property of uplink-downlink duality, the virtual uplink SINR_n^0 derivation denoted by $\overline{\text{SINR}}_n^0$ has the same structure as SINR_n^0 expression, however, $P_{(co)n}^0$ is replaced by $\overline{P}_{(co)n}^0$, with

$$\overline{P}_{(co)n}^0 = \sum_{\substack{n'=1 \\ n' \neq n}}^{N_0} \left\| \sum_{m=1}^{M_0} \sqrt{p_{n'}^0} \mathbf{u}_{mn'} * \mathbf{h}_{mn'}^{01} \right\|^2. \quad (35)$$

Since \mathbf{p}_n^0 is a non-negative vector, it can be re-written in the new form

$$\exp(\xi_n) = p_n^0. \quad (37)$$

On this basis, the inversion of $\overline{\text{SINR}}_n^0$ can be computed as

$$\left(\overline{\text{SINR}}_n^0 \right)^{-1} = \Delta_n + \nabla_n \exp(-\xi_n), \quad (38)$$

where Δ_n is defined as in (36) and

$$\nabla_n = \frac{P_{(cross)n}^{*0} + \|\mathbf{n}_M\|^2}{\left| \left(\sum_{m=1}^{M_0} \mathbf{u}_{mn} * \mathbf{h}_{mn}^{01} \right) [\alpha] \right|^2}. \quad (39)$$

Without loss of generality, the problem OP_2 is reformulated into a more tractable formulation such as

$$\begin{aligned} \text{OP}_3: \min_{\{\xi_n\}_{n=1}^{N_0}} \quad & \sum_{n=1}^{N_0} \exp(\xi_n) \\ \text{s.t.} \quad & \log(\Delta_n + \nabla_n \exp(-\xi_n)) \leq \log \frac{1}{\gamma_n^0}, \\ & \left\| \sum_{m=1}^{M_0} \mathbf{u}_{mn} * \mathbf{h}_{mj}^{01} \right\|^2 \exp(\xi_n) \leq P_{(tol)j}^{01}. \end{aligned} \quad (40)$$

Indeed, the problem OP_3 is convex and it is solvable by use of Lagrange multiplier method [29]. Considering the relationship between OP_2 and OP_3 , it is clear that the optimal solution of OP_2 can be calculated according to that of OP_3 , i.e. $p_n^{*0} = \exp(\xi_n^*)$ where ξ_n^* is the optimal solution of OP_3 .

In the continuity, following Lagrange multiplier method, let $\{\mu_n\}$ and $\{\lambda_n\}$ be the dual variables associated with the SINR and interference constraints, respectively. After some mathematical manipulations, the Lagrangian function of OP_3 can be given by

$$\begin{aligned} \mathcal{L}(\{\xi_n\}, \{\mu_n\}, \{\lambda_n\}) = & \sum_{n=1}^{N_0} \exp(\xi_n) \\ & + \sum_n \mu_n \left(\log(\Delta_n + \nabla_n \exp(-\xi_n)) - \log \frac{1}{\gamma_n^0} \right) \\ & + \sum_{n=1}^{N_0} \lambda_n \left(\left\| \sum_{m=1}^{M_0} \mathbf{u}_{mn} * \mathbf{h}_{mj}^{01} \right\|^2 \exp(\xi_n) - P_{(tol)j}^{01} \right). \end{aligned} \quad (41)$$

For convenience, we focus on the following simplified form of (41)

$$\begin{aligned} \mathcal{L}_n(\xi_n, \mu_n, \lambda_n) = & \exp(\xi_n) + \mu_n \log(\Delta_n + \nabla_n \exp(-\xi_n)) \\ & + \lambda_n \left\| \sum_{m=1}^{M_0} \mathbf{u}_{mn} * \mathbf{h}_{mj}^{01} \right\|^2 \exp(\xi_n). \end{aligned} \quad (42)$$

Accordingly, the dual function and the dual problem can explicitly be formulated as (43) and (44), respectively

$$\mathcal{D}(\{\xi_n\}, \{\mu_n\}, \{\lambda_n\}) = \sum_{n=1}^{N_0} \min_{\xi_n} \mathcal{L}_n(\xi_n, \mu_n, \lambda_n) \quad (43)$$

$$- \sum_{n=1}^{N_0} \mu_n \left(\log \frac{1}{\gamma_n^0} \right) - \sum_{n=1}^{N_0} \lambda_n (P_{(tol)j}^{01}),$$

$$\begin{aligned} \text{OP}_4: \max_{\{\mu_n\}, \{\lambda_n\}} \quad & \mathcal{D}(\{\mu_n\}, \{\lambda_n\}) \\ \text{s.t.} \quad & \{\mu_n\} \geq 0, \{\lambda_n\} \geq 0, \forall n \end{aligned} \quad (44)$$

It is a fact that the problem OP_3 is a convex optimization problem, thus strong duality holds, i.e. the duality gap between primal problem and dual problem is zero. According

$$\Delta_n = \frac{\sum_{l \neq \alpha}^{2L-1} \left| \left(\sum_{m=1}^{M_0} \mathbf{u}_{mn} * \mathbf{h}_{mn}^0 \right) [l] \right|^2 + \sum_{\substack{n'=1 \\ n' \neq n}}^{N_0} \left\| \sum_{m=1}^{M_0} \mathbf{u}_{mn} * \mathbf{h}_{mn'}^0 \right\|^2}{\left| \left(\sum_{m=1}^{M_0} \mathbf{u}_{mn} * \mathbf{h}_{mn}^0 \right) [\alpha] \right|^2}. \quad (36)$$

to Karush-Kuhn-Tucker condition, the optimal transmit power can be obtained through the first derivative of the Lagrangian function with respect to ξ_n as

$$\frac{\partial \mathcal{L}_n(\xi_n, \mu_n, \lambda_n)}{\partial \xi_n} = 0. \quad (45)$$

Specifically, the optimal solution p_n^{*0} can be achieved by the closed-form derivation

$$p_n^{*0} = \exp(\xi_n^*) = \frac{2\mu_n \nabla_n \lambda_n^{-1} \left\| \sum_{m=1}^{M_0} \mathbf{u}_{mn} * \mathbf{h}_{mj}^{01} \right\|^{-2}}{\left(\nabla_n + \sqrt{\nabla_n^2 + \frac{4\nabla_n \Delta_n \mu_n}{\lambda_n \left\| \sum_{m=1}^{M_0} \mathbf{u}_{mn} * \mathbf{h}_{mj}^{01} \right\|^2}} \right)}. \quad (46)$$

The final step in this method is to provide optimal Lagrangian multipliers, i.e. μ_n and λ_n by solving the dual problem OP₄. In this way, the optimal solution of OP₃ is obtained once $\exp(\xi_n)$, μ_n and λ_n are iteratively updated until convergence. The subgradient iteration algorithm is then applied to update the Lagrangian multipliers as

$$\mu_n(t) = [\mu_n(t-1) + \nu_n(t) X_1]^+, \quad (47)$$

$$\lambda_n(t) = [\lambda_n(t-1) + \kappa_n(t) X_2]^+, \quad (48)$$

where $\nu_n(t)$ and $\kappa_n(t)$ are step sizes, while X_1 and X_2 are defined as

$$X_1 = \log(\Delta_n + \nabla_n \exp(-\xi_n)) - \log \frac{1}{\gamma_n^0}, \quad (49)$$

$$X_2 = \left\| \sum_{m=1}^{M_0} \mathbf{u}_{mn} * \mathbf{h}_{mj}^{01} \right\|^2 \exp(\xi_n) - P_{(tol)j}^{01}. \quad (50)$$

The subgradient iterative algorithm is ensured to converge to the optimal value with a sufficiently small step size [29].

V. WORST-CASE ROBUST OPTIMIZATION FOR TR FEMTOCELL NETWORK

In this section, we extend the downlink power minimization problem for the TR femtocell by considering imperfect CSI. It is worth noting that this work considers for the first time the worst-case robust optimization for TR femtocell network.

Accounting for error model, we assume that the maximum error quantity of the femtocell can be known, such that the imperfect CIR model can be referred to as

$$\hat{\mathbf{h}}_{ij}^1 = \mathbf{h}_{ij}^1 + \mathbf{e}_{ij}^1, \quad (52)$$

where \mathbf{e}_{ij}^1 represents a channel uncertainty defined by a feasible set as

$$\mathcal{F}_{ij}^1 = \left\{ \mathbf{e}_{ij}^1 \in \mathbb{C}^{L \times 1} : \|\mathbf{e}_{ij}^1\|^2 \leq \psi \|\mathbf{h}_{ij}^1\|^2 \right\}, \quad (53)$$

and ψ is named as error factor. We also suppose that \mathbf{h}_{ij}^1 and \mathbf{e}_{ij}^1 are identically and independently distributed variables. Under the influence of CEE, we devise the robust optimization methodologies to guarantee the QoS requirement. Following the worst-case approach, the power allocation design of the femtocells may be formulated as

$$\begin{aligned} \text{OP}_5: \min_{\mathbf{p}^1} \quad & \max_{\mathbf{e}_{in}^{10}} \sum_{j=1}^{N_1} \left(\sum_{n=1}^{N_0} \left\| \sum_{i=1}^{M_1} \hat{\mathbf{g}}_{ij} * \mathbf{h}_{in}^{10} \right\|^2 p_j^1 \right) \\ \text{s.t.} \quad & \min_{\mathbf{e}_{ij}^1, \mathbf{e}_{ij'}^1} \text{SINR}_j^1 \left(L, \mathbf{p}^1, \{\hat{\mathbf{g}}_{ij}^1\}_{i=1, j=1}^{M_1, N_1}, P_{(tol)j}^{01} \right) \geq \gamma_j^1 \\ & (\mathbf{e}_{in}^{10} \in \mathcal{F}_{in}^{10}, \mathbf{e}_{ij}^1 \in \mathcal{F}_{ij}^1, \mathbf{e}_{ij'}^1 \in \mathcal{F}_{ij'}^1). \end{aligned} \quad (54)$$

Unluckily, the problem OP₅ is intractable since the objective function and constraint include the convolution operator. However, it can be transformed into a convex one by approximating the latters. Indeed, one can see that it is challenging to obtain an exact closed-form SINR expression in the constraint.

To tackle this problem, we apply an approximation presented as (51) in which $\mathcal{P}l_{(sig)j}^1$, $\mathcal{P}u_{(isi)j}^1$ and $\mathcal{P}u_{(co)j}^1$ are the worst-case lower-bound of central signal power, the worst-case upper-bound of ISI power, and worst-case upper-bound of co-tier interference power, respectively.

$$\mathcal{P}l_{(sig)j}^1 = \min_{\mathbf{e}_{ij}^1 \in \mathcal{F}_{ij}^1} \left\| \sum_{i=1}^{M_1} (\hat{\mathbf{g}}_{ij} * \mathbf{h}_{ij}^1) [L] \sqrt{p_j^1} \right\|^2, \quad (55)$$

$$\mathcal{P}u_{(isi)j}^1 = \max_{\mathbf{e}_{ij}^1 \in \mathcal{F}_{ij}^1} \left\| \sum_{i=1}^{M_1} \hat{\mathbf{g}}_{ij} * \mathbf{h}_{ij}^1 \right\|^2 - \mathcal{P}l_{(sig)j}^1, \quad (56)$$

$$\mathcal{P}u_{(co)j}^1 = \max_{\mathbf{e}_{ij'}^1 \in \mathcal{F}_{ij'}^1} \sum_{j'=1}^{N_1} \left\| \sum_{i=1}^{M_1} \sqrt{p_{j'}^1} \hat{\mathbf{g}}_{ij'} * \mathbf{h}_{ij}^1 \right\|^2, \quad (57)$$

where $\hat{\mathbf{g}}_{ij}$ is the beamformer corresponding to the estimated channel $\hat{\mathbf{h}}_{ij}^1$, and it has a similar structure to \mathbf{g}_{ij} shown in (22). Note that the derivation of $\mathcal{P}u_{(isi)j}^1$ can be expressed as a subtraction between the upper-bound of the power of all taps and the lower-bound of the power of central tap. Our aim is to derive such these boundaries into formulations that can be expressed in term of estimated values solely, e.g. $\hat{\mathbf{g}}_{ij}$, $\hat{\mathbf{h}}_{ij}^1$.

$$\min_{\mathbf{e}_{ij}^1, \mathbf{e}_{ij'}^1} \text{SINR}_j^1 \left(\beta, \mathbf{p}^1, \{\hat{\mathbf{g}}_{ij}^1\}_{i=1, j=1}^{M_1, N_1}, P_{(tol)j}^{01} \right) \approx \frac{\mathcal{P}l_{(sig)j}^1(p_j^1, \hat{\mathbf{g}}_{ij}^1)}{\mathcal{P}u_{(isi)j}^1(p_j^1, \hat{\mathbf{g}}_{ij}^1) + \mathcal{P}u_{(co)j}^1(\{p_{j'}^1, \hat{\mathbf{g}}_{ij'}^1\}_{j'=1, j' \neq j}^{N_1}) + P_{(tol)j}^{01} + \|\mathbf{n}_F[L]\|^2}. \quad (51)$$

A. Worst-case lower-bound of signal power component

This part of the paper is dedicated to the derivation of the worst-case lower-bound of signal power given in equation (55).

With an erroneous channel estimation, the power of the central tap at the intended user becomes

$$\begin{aligned} & \left| \sum_{i=1}^{M_1} (\hat{\mathbf{g}}_{ij}^1 * \mathbf{h}_{ij}^1)[L] \right|^2 \\ &= \frac{\left| \sum_{i=1}^{M_1} \left(\sum_{l=1}^L h_{ij}^1[l] h_{ij}^{*1}[l] + \sum_{l=1}^L e_{ij}^1[l] h_{ij}^{*1}[l] \right) \right|^2}{\sum_{i=1}^{M_1} \|\hat{\mathbf{h}}_{ij}^1\|^2} \\ &= \frac{\left| \sum_{i=1}^{M_1} \left(\|\mathbf{h}_{ij}^1\|^2 + (\mathbf{e}_{ij}^1)^H \mathbf{h}_{ij}^1 \right) \right|^2}{\sum_{i=1}^{M_1} \|\hat{\mathbf{h}}_{ij}^1\|^2}, \end{aligned} \quad (58)$$

where we have

$$\|\hat{\mathbf{h}}_{ij}^1\|^2 = \|\mathbf{h}_{ij}^1\|^2 + \|\mathbf{e}_{ij}^1\|^2 + 2\Re\{(\mathbf{e}_{ij}^1)^H \mathbf{h}_{ij}^1\}. \quad (59)$$

One can evaluate that while $\|\hat{\mathbf{h}}_{ij}^1\|^2$ is fixed, if $\|\mathbf{e}_{ij}^1\|^2$ increases then $\|\mathbf{h}_{ij}^1\|^2$ decreases. Considering (58), the increasing level of $(\mathbf{e}_{ij}^1)^H \mathbf{h}_{ij}^1$ is generally lower than the decreasing level of $\|\mathbf{h}_{ij}^1\|^2$. Therefore, the CEE effect monotonically reduces the power of desired signal, and the power focalization is decreased. *Lemma 2* below determines $\mathcal{P}l_{(sig)j}^1$ based on (58).

Lemma 2. *The worst-case lower-bound on the signal power component can be stated as*

$$\mathcal{P}l_{(sig)j}^1 = \left| \sum_{i=1}^{M_1} (\hat{\mathbf{g}}_{ij}^1 * \hat{\mathbf{h}}_{ij}^1)[L] \right|^2 \frac{p_j^1}{(1 - \sqrt{\psi})^2}. \quad (60)$$

Proof: The proof is listed in Appendix B. ■

B. Worst-case upper-bound on the ISI power component

In order to find out worst-case upper-bound on the ISI term, the maximum of Euclidean norm of $\sum_{i=1}^{M_1} \hat{\mathbf{g}}_{ij}^1 * \mathbf{h}_{ij}^1$,

i.e. $\max_{\mathbf{e}_{ij}^1 \in \mathcal{F}_{ij}^1} \left\| \sum_{i=1}^{M_1} \hat{\mathbf{g}}_{ij}^1 * \mathbf{h}_{ij}^1 \right\|^2$ needs to be discovered first. This problem is non-trivial since only the knowledge of the norm constraint of the estimation error is available, see (53). Fortunately, thanks to Young's inequality [25], [eq (3.9.4) [30]] the upper-bound can be derived. In this vein, the norm of

convolution between the given two vectors can be bounded by Young's inequality as

$$\begin{aligned} & \left\| \sum_{i=1}^{M_1} \hat{\mathbf{g}}_{ij}^1 * \mathbf{h}_{ij}^1 \right\|^2 \leq \hat{c} \sum_{i=1}^M \|\mathbf{h}_{ij}^1\|^2 \|\hat{\mathbf{g}}_{ij}^1\|_1^2 \\ & + \hat{c} \sum_{i=1}^{M_1} \sum_{\substack{i'=1 \\ i' \neq i}}^{M_1} \|\mathbf{h}_{ij}^1\| \|\hat{\mathbf{g}}_{ij}^1\|_1 \|\mathbf{h}_{i'j}^1\| \|\hat{\mathbf{g}}_{i'j}^1\|_1, \end{aligned} \quad (61)$$

where $\|\cdot\|_1$ denotes the l_1 -norm and \hat{c} is a constant. One can see that the resulting boundary can be computed as a function of the norm of these two vectors only. Concerning the worst possible error case, based on the defined feasible set given in (53), we have

$$\begin{aligned} & \max_{\mathbf{e}_{ij}^1 \in \mathcal{F}_{ij}^1} \left\| \sum_{i=1}^{M_1} \hat{\mathbf{g}}_{ij}^1 * \mathbf{h}_{ij}^1 \right\|^2 = \hat{c} \sum_{i=1}^{M_1} \frac{\|\hat{\mathbf{h}}_{ij}^1\|^2 \|\hat{\mathbf{g}}_{ij}^1\|_1^2}{(1 - \sqrt{\psi})^2} \\ & + \hat{c} \sum_{i=1}^{M_1} \sum_{\substack{i'=1 \\ i' \neq i}}^{M_1} \frac{\|\hat{\mathbf{h}}_{ij}^1\| \|\hat{\mathbf{g}}_{ij}^1\|_1 \|\hat{\mathbf{h}}_{i'j}^1\| \|\hat{\mathbf{g}}_{i'j}^1\|_1}{(1 - \sqrt{\psi})^2}. \end{aligned} \quad (62)$$

On the other hand, the objective function and $\mathcal{P}u_{(isi)j}^1$ also contain the worst-case boundary of the norm of convolution between two vectors. It is a fact that the tight degree of the boundary plays an important role in limiting the waste of the transmit power allocation. For a long time, the designation of a value to the constant \hat{c} in (61) that can improve the tightness of Young's inequality was a challenge for researchers. Eventually, Beckner [31] provided the best possible constant \hat{c} and the work in [32] generalized Young's inequality, the value of \hat{c} designed by [31], [32] has no effect in the case considered in our work, i.e. \hat{c} is equal to 1. This motivates us to derive a tighter worst-case upper-bound on the ISI component through *Lemma 3*.

Lemma 3. *Considering the worst-case boundary of the norm of convolution between two vectors, we introduce a new formulation as follows*

$$\begin{aligned} & \max_{\mathbf{e}_{ij}^1 \in \mathcal{F}_{ij}^1} \left\| \sum_{i=1}^{M_1} \hat{\mathbf{g}}_{ij}^1 * \mathbf{h}_{ij}^1 \right\|^2 \\ &= \sum_{i=1}^{M_1} \left\| \hat{\mathbf{g}}_{ij}^1 * \tilde{\mathbf{h}}_{ij}^{*1} \right\|^2 + \left| \sum_{i=1}^{M_1} \sum_{\substack{i'=1 \\ i' \neq i}}^{M_1} (\hat{\mathbf{g}}_{ij}^1 * \tilde{\mathbf{h}}_{ij}^{*1})^H (\hat{\mathbf{g}}_{i'j}^1 * \tilde{\mathbf{h}}_{i'j}^{*1}) \right|. \end{aligned} \quad (63)$$

in which,

$$\tilde{\mathbf{h}}_{ij}^{*1} = \frac{(\Phi_{ij}^{*1}) \|\hat{\mathbf{h}}_{ij}^1\|}{(1 - \sqrt{\psi})}, \quad (64)$$

where Φ_{ij}^{*1} can be obtained by computing the orthonormal eigenvector corresponding to the largest eigenvalue of the matrix $\left(\hat{\mathbf{G}}_{ij} (\hat{\mathbf{G}}_{ij})^H \frac{\|\hat{\mathbf{h}}_{ij}^1\|^2}{(1 - \sqrt{\psi})^2} \right)$, and

$$\hat{\mathbf{G}}_{ij} \in \mathbb{C}^{(2L-1) \times L} = \begin{bmatrix} \hat{g}_{ij}[1] & 0 & 0 & 0 & 0 \\ \hat{g}_{ij}[2] & \hat{g}_{ij}[1] & \cdots & \vdots & \vdots \\ \hat{g}_{ij}[3] & \hat{g}_{ij}[2] & \cdots & 0 & 0 \\ \vdots & \hat{g}_{ij}[3] & \cdots & \hat{g}_{ij}[1] & 0 \\ \hat{g}_{ij}[L-1] & \vdots & \cdots & \hat{g}_{ij}[2] & \hat{g}_{ij}[1] \\ \hat{g}_{ij}[L] & \hat{g}_{ij}[L-1] & \vdots & \vdots & \hat{g}_{ij}[2] \\ 0 & \hat{g}_{ij}[L] & \cdots & \hat{g}_{ij}[L-2] & \vdots \\ 0 & 0 & \cdots & \hat{g}_{ij}[L-1] & \hat{g}_{ij}[L-2] \\ \vdots & \vdots & \vdots & \hat{g}_{ij}[L] & \hat{g}_{ij}[L-1] \\ 0 & 0 & 0 & \cdots & \hat{g}_{ij}[L] \end{bmatrix}. \quad (65)$$

Proof: Please refer to Appendix C. ■

Accordingly, the proposed upper-bound on $P_{(isi)j}^1$ can be calculated as

$$\mathcal{P}u_{(isi)j}^1 = \sum_{i=1}^{M_1} \left\| \sqrt{p_j^1} \hat{\mathbf{g}}_{ij} * \tilde{\mathbf{h}}_{ij}^{*1} \right\|^2 - \mathcal{P}l_{(sig)j}^1 \quad (66)$$

$$+ \left| \sum_{i=1}^{M_1} \sum_{\substack{i'=1 \\ i' \neq i}}^{M_1} \left(\sqrt{p_j^1} \hat{\mathbf{g}}_{ij} * \tilde{\mathbf{h}}_{ij}^{*1} \right)^H \left(\sqrt{p_j^1} \hat{\mathbf{g}}_{i'j} * \tilde{\mathbf{h}}_{i'j}^{*1} \right) \right|.$$

C. Worst-case upper bound on the co-tier interference and objective function

Similarly, the upper bound on the co-tier interference may be presented as follows

$$\mathcal{P}u_{(co)j}^1 = \sum_{\substack{j'=1 \\ j' \neq j}}^{N_1} \left(\sum_{i=1}^{M_1} \left\| \hat{\mathbf{g}}_{ij'} * \tilde{\mathbf{h}}_{ij'}^{*1} \right\|^2 p_{j'}^1 \right) + \sum_{\substack{j'=1 \\ j' \neq j}}^{N_1} \left| \sum_{i=1}^{M_1} \sum_{\substack{i'=1 \\ i' \neq i}}^{M_1} \left(\hat{\mathbf{g}}_{ij'} * \tilde{\mathbf{h}}_{ij'}^{*1} \right)^H \left(\hat{\mathbf{g}}_{i'j'} * \tilde{\mathbf{h}}_{i'j'}^{*1} \right) p_{j'}^1 \right|. \quad (67)$$

and the upper bound on the objective function is developed as

$$\begin{aligned} & \max_{\mathbf{e}_{in}^{10} \in \mathcal{F}_{in}^{10}} \sum_{j=1}^{N_1} \left(\sum_{n=1}^{N_0} \left\| \sum_{i=1}^{M_1} \hat{\mathbf{g}}_{ij} * \tilde{\mathbf{h}}_{in}^{*10} \right\|^2 p_j^1 \right) \\ &= \sum_{j=1}^{N_1} \left(\sum_{n=1}^{N_0} \sum_{i=1}^{M_1} \left\| \hat{\mathbf{g}}_{ij} * \tilde{\mathbf{h}}_{in}^{*10} \right\|^2 p_j^1 \right) \\ &+ \sum_{j=1}^{N_1} \left| \sum_{n=1}^{N_0} \sum_{i=1}^{M_1} \sum_{\substack{i'=1 \\ i' \neq i}}^{M_1} \left(\hat{\mathbf{g}}_{ij} * \tilde{\mathbf{h}}_{in}^{*10} \right)^H \left(\hat{\mathbf{g}}_{i'j} * \tilde{\mathbf{h}}_{i'n}^{*10} \right) p_j^1 \right| \\ &= \Omega(\mathbf{p}^1). \end{aligned} \quad (68)$$

TABLE II
ITU INDOOR OFFICE [33]

Tap	Relative Delay (ns)	Average Power (dBm)
1	0	0
2	50	-3
3	100	-10
4	170	-18
5	290	-26
6	310	-32

TABLE III
ITU VEHICULAR [33]

Tap	Relative Delay (ns)	Average Power (dBm)
1	0	0
2	310	-1
3	710	-9
4	1090	-10
5	1730	-15
6	2510	-20

Following the worst-case approach and results from (83) and (66), (67), and (68), the problem OP_6 can be approximately relaxed as problem OP_6

$$\begin{aligned} \text{OP}_6: \quad & \min_{\mathbf{p}^1} \quad \Omega(\mathbf{p}^1) \\ \text{s.t.} \quad & \frac{\mathcal{P}l_{(sig)j}^1}{\mathcal{P}u_{(isi)j}^1 + \mathcal{P}u_{(co)j}^1 + P_{(tol)j}^{01} + \|\mathbf{n}_F\|^2} \geq \gamma_j^k. \end{aligned} \quad (69)$$

This problem can be solved by the use of a similar approach adopted to tackle OP_1 .

VI. NUMERICAL RESULTS

The impact of the proposed power allocation strategy on the system performance is analyzed in this section. Without other statements, the system parameters are set following the ITU-R channel model [33] which is applicable for vehicular and indoor communication environments where the macrocell and femtocell are implemented, respectively.

In the HetNet, the radii of MBS and FBS are $d_m = 300$ m and $d_f = 30$ m respectively. FBS is uniformly distributed in a circle of $d_{mf} = 100$ m far from MBS. MUs and FUs are also uniformly distributed in the served areas of MBS and FBS, respectively. Specifically, the macrocell, femtocell and the cross-tier channels are considered as the ITU vehicular (Table II), the ITU indoor (Table III), the ITU outdoor to indoor (Table IV) models, respectively. Moreover, we assume that

- The outdoor link pathloss exponent is set to 4, thus each tap of MBS-to-MU links is $\mathcal{CN}(0, |\mathbf{h}_{mn}^0[l]|^2)$ where $|\mathbf{h}_{mn}^0[l]|^2 = \sigma_{0mn,l}^2/d_{0n}^4$ and d_{0n} is the distance between MBS and the n -th MU ($0 \leq d_{0n} \leq d_m$).
- The indoor link pathloss exponent is set to 3, thus each tap of FBS-to-FU links is $\mathcal{CN}(0, |\mathbf{h}_{ij}^1[l]|^2)$ where $|\mathbf{h}_{ij}^1[l]|^2 = \sigma_{1ij,l}^2/d_{1j}^3$ and d_{1j} is the distance between FBS and the j -th FU ($0 \leq d_{1j} \leq d_f$).
- The outdoor-to-indoor link pathloss exponent is set to 3.5, thus each tap of MBS-to-FU links is $\mathcal{CN}(0, |\mathbf{h}_{mj}^{01}[l]|^2)$

TABLE IV
ITU OUTDOOR TO INDOOR AND PEDESTRIAN [33]

Tap	Relative Delay (ns)	Average Power (dBm)
1	0	0
2	110	-9.7
3	190	-19.2
4	410	-22.8

TABLE V
IMPORTANT PARAMETERS

Parameters	System values
Number of taps, L	6
Number of antennas at MBS, M_0	4
Number of antennas at FBS, M_1	4
Number of users at MBS, N_0	2
Number of users at FBS, N_1	2-4
Tolerable level of cross-interference, $P_{(tol)}^{01}$	-10 dBm
Bandwidth, W	20 MB

where $|\mathbf{h}_{mj}^{01}[l]|^2 = \sigma_{01mj,l}^2/d_{01j}^{3.5}$ and d_{01j} is the distance between MBS and the j -th FU ($0 \leq d_{01j} \leq d_f$).

- The indoor-to-outdoor links are assumed to be similar to the outdoor-to-indoor links.

It is worth noting that there exist no correlations between the channels and between their taps.

For convenience, we set the SINR thresholds for FBS as $\{\gamma_j^1\}_{j=1}^{N_1} = \gamma_F$ and for MBS as $\{\gamma_n^0\}_{n=1}^{N_0} = \gamma_M$. In addition, the Gaussian noise power is set to 10^{-12} W and other parameters are adjusted as listed in Table VI.

A. The Proposed Power Allocation Strategy

In Fig. 3, we investigate the transmit power of the HetNet system with the proposed optimization approach, and the scheme using centralized manner. The simulation is carried out with 1000 random locations of MBS, FBS and users in the considered HetNet environment. Since MUs are frequently located far from its own base station, the distance between MBS and MUs is much larger compared with the distance between FBS and FUs. Therefore, the amount of transmit power allocated for MUs constitutes a major part of the total

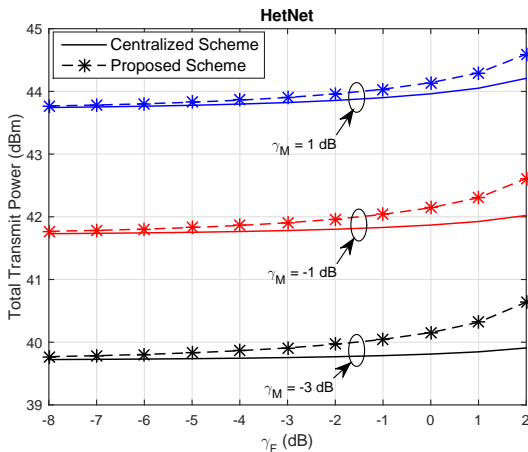


Fig. 3. Performance of power allocation schemes.

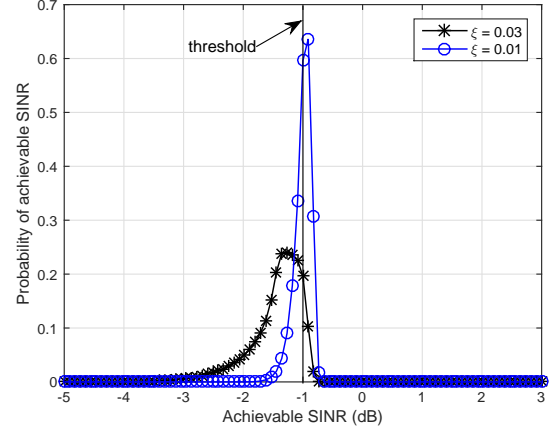


Fig. 4. Impact of imperfect $\{\mathbf{h}_{in}^{10}\}_{j=1, n=1}^{N_1, N_0}$ on the performance at a MU.

transmit power of HetNet. As a result, the total transmit power slightly increases when the SINR threshold of FUs scales up. Fig. 3 also shows the comparison between the centralized and the proposed approaches. In more details, the power gap at $\gamma_F = 2$ dB is roughly 0.6 dB, 0.5 dB and 0.4 dB in cases of $\gamma_M = 1$ dB, -1 dB and -3 dB, respectively. Furthermore, the gap scales up as the SINR threshold of FUs increases. This is because the FBS aims at minimizing the interference to MUs, instead of solely minimizing the transmit power as in the case of centralized approach. More specifically, the proposed scheme sacrifices an additional amount of transmit power for (i) a much smaller amount of required signaling information and (ii) a reduced interference to MU. Note that only $\{P_{(cross)n}^{01}\}_{n=1}^{N_0}$ is sent via backhaul to the macrocell instead of \mathbf{p}^* , $\{\mathbf{h}_{ij}^1\}_{i=1, j=1}^{M_1, N_1}$ and $\{\mathbf{h}_{in}^{10}\}_{j=1, n=1}^{N_1, N_0}$, the signaling overhead is significantly reduced. Indeed, based on Fig. 3, one can conclude that the proposed optimization algorithm can achieve tight results to the centralized strategy which validates and verifies our strategy.

Moreover, in practice, obtaining the perfect information of cross channels, such as $\{\mathbf{h}_{in}^{10}\}_{i=1, n=1}^{M_1, N_0}$ and $\{\mathbf{h}_{mj}^{01}\}_{m=1, j=1}^{M_0, N_1}$, is a challenge. Although many previous works [23], [24], [28] assume that the information is available at the base station or the computation node, this motivates us to further consider the impact of imperfect $\{\mathbf{h}_{in}^{10}\}_{j=1, n=1}^{N_1, N_0}$ on the SINR performance achieved at MUs. The latter represents the case in which FBS imperfectly estimate the CSI of $\{\mathbf{h}_{in}^{10}\}_{j=1, n=1}^{N_1, N_0}$, and then it sends the "inaccurate" information of minimized interference to MBS. In this concern, we use a general imperfect channel model as $\hat{\mathbf{h}}_{in}^{10} = \mathbf{h}_{in}^{10} + \mathbf{e}_{in}^{10}$, where \mathbf{e}_{in}^{10} is a channel uncertainty and $\|\mathbf{e}_{in}^{10}\|_2^2 \leq \xi \mathbf{h}_{in}^{10}$. In fact, the inexact information of $\{\mathbf{h}_{in}^{10}\}_{j=1, n=1}^{N_1, N_0}$ might lead to the fact that the achieved SINR performance at each MU is not guaranteed to meet the preset threshold. In Fig. 4, the impact of imperfect CSI is shown in terms of the probability of the achievable SINR at a MU. As expected, given the threshold of -1 dB, it is clear that the outage probability increases when the error component scales up.

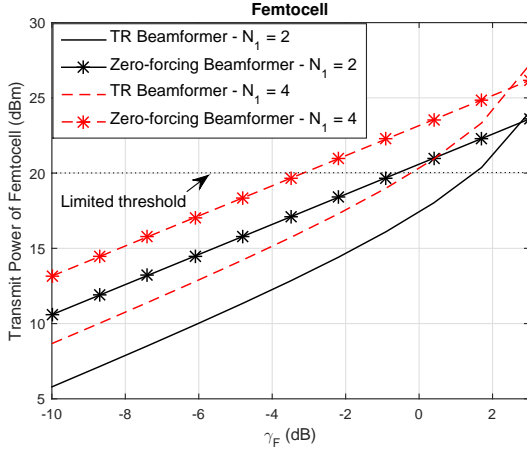


Fig. 5. A comparison between TR and zero-forcing.

B. Comparison between TR and zero-forcing techniques

In Fig. 5, we compare the effectiveness of TR-based beamformer with that of zero-forcing-based beamformer (*Algorithm 1*). Concerning channels, the ITU-R indoor model is still utilized, however, we arrange a distance of 15 meters between FBS and FUs. From Fig. 5, it is visible that for a transmit power range lower than 23 dBm and 25 dBm for cases of $N_1 = 2$ users and $N_1 = 4$ users, respectively, TR beamforming outperforms zero-forcing one and converse holds for the entire transmit power regions. Specifically, it can be explained that zero-forcing scheme mainly deals with canceling the ISI, co-tier interference and cross-tier interference, whereas TR technique aims at both focusing signal power on the central tap, and reducing the ISI and co-tier interferences. As a result, the interference is ineliminable completely in TR-applying systems, and the interference power increases as transmit power scales up. Therefore, there exist working ranges in which either TR or zero-forcing techniques can dominate the other one regarding SINR metric. In practice, however, FBS is a low-power cellular station whose transmit power is limited to 20dBm in order to curb the effects of co- and cross-tier interferences [1]. Indeed, in perspective of a small-cell system configured with a limited level of transmit power, such as femtocell operating environments, it can be concluded that the TR technique is more desirable than the zero-forcing.

C. Worst-case Optimization Problem and Performance of Proposed Upper-bounds

In Section V, we have proposed a novel worst-case upper-bound to provide a greater solution to the robust downlink power allocation for the TR femtocell. First, for simplicity, we observe the term $\left\| \sum_{i=1}^{M_1} \hat{\mathbf{g}}_{ij} * \mathbf{h}_{ij}^1 \right\|^2$ to evaluate the performance of the proposed boundary and Young's inequality-based boundary. Simulations are carried out in indoor channels with a fixed pathloss similar to the prior investigation. Fig. 6 clearly demonstrates that the proposed boundary is approximately 5dB tighter than Young's inequality-based boundary at $M_1 = 4$ for both cases of error factor $\psi = 0.05, 0.1$.

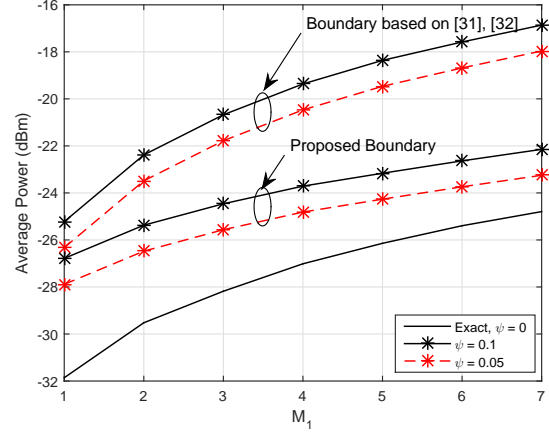


Fig. 6. A comparison between worst-case upper-bounds.

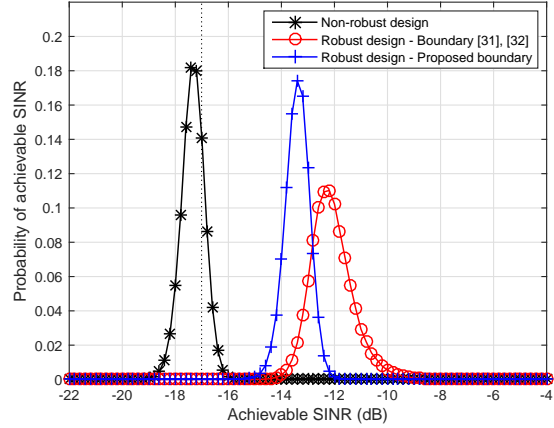


Fig. 7. Probability distribution per a femtocell user.

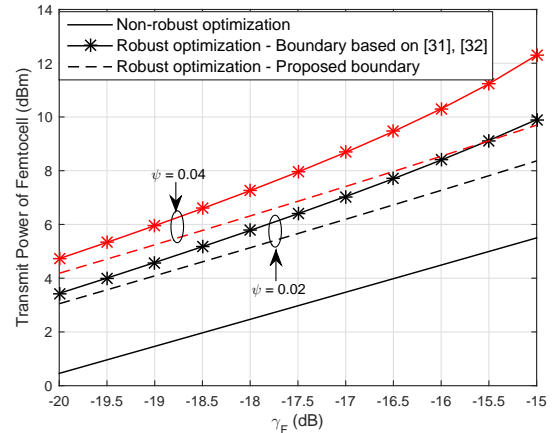


Fig. 8. Transmit power of femtocell with worst-case upper-bounds.

Concerning the worst case robust design, Fig. 7 and Fig. 8 demonstrate the transmission power in terms of worst-case approaches using: (i) the Young's inequality-based boundary as well as (ii) the proposed boundary, under similar error conditions. In more details, Fig. 7 exhibits the probability distribution of achievable SINR per FU obtained by non-robust design (OP₁) and robust design (OP₆). This result is achieved by use of 100000 randomly generated realizations for the simulation. For the channel error factor $\psi = 0.04$, our simulation shows that two robust designs can keep the outage probability equal to 0 by accounting the worst possible error case. Nevertheless, the probability distribution of the design employing the proposed boundary is closer to the preset threshold than that of Young's inequality-based design. It can be explained that FBS can save the radiated energy in obtaining the same desired SINR performance when applying the proposed boundary.

Moreover, as a reference, we plot the average transmit power of non-robust and robust manners in Fig. 8 and exhibit the amount of additional power that is needed to achieve a zero outage probability. It can be concluded that the advantage of our boundary makes the transmit power allocation more effective in the *worst-case approach* by curbing the waste of power transmission.

VII. CONCLUSION

In this paper, we propose the application of TR technique to femtocell networks, and a novel power allocation scheme for the considered HetNet in which the backhaul connection provides only a limited throughput for signaling exchange. In perfect channel estimation cases, we tackle the beamformer designs and optimization problems of downlink power control for both macrocell and femtocell over frequency selective fading channels. Our analysis shows that the proposed allocation schemes require a higher increment in transmit power compared to the conventional approach but demands a lower amount of signaling exchange between the MBS and FBS. This important advantage makes our approach very promising to deal with limited backhaul connection drawbacks. Furthermore, under imperfect CSI assumption, we tackle the robust design following the worst-case approach. To relax the original formulation into a solvable convex problem, the worst-case boundaries of concerning components are derived. In particular, we propose the novel tighter worst-case upper-bound of the ISI, co-tier interference and objective function to improve the system performance. Moreover, numerical results demonstrate that the TR technique outperforms the zero-forcing beamforming over femtocell working environments.

APPENDIX A PROOF OF LEMMA 1

To solve this problem OP₁, we start with introducing a new parameter for the objective function as follows

$$\sum_{j=1}^{N_1} \left(\sum_{n=1}^{N_0} \left\| \sum_{i=1}^{M_1} \mathbf{g}_{ij} * \mathbf{h}_{in}^{10} \right\|^2 p_j^1 \right) = \hat{\boldsymbol{\eta}}^T \mathbf{p}^1, \quad (70)$$

where $\hat{\boldsymbol{\eta}}$ are defined in Lemma 1.

Next, the expression of SINR_j¹ in (14) can be re-written as

$$\begin{aligned} \text{SINR}_j^1 \left(L, \mathbf{p}^1, \{ \mathbf{g}_{ij}^1 \}_{i=1, j=1}^{M_1, N_1}, P_{(cross)j}^1 \right) \\ = \frac{\left(\left| \left(\sum_{i=1}^{M_1} \mathbf{g}_{ij} * \mathbf{h}_{ij}^1 \right) [L] \right|^2 - \gamma_j^1 \sum_{l=1, l \neq L}^{2L-1} \left| \left(\sum_{i=1}^{M_1} \mathbf{g}_{ij} * \mathbf{h}_{ij}^1 \right) [l] \right|^2 \right) p_j^1}{P_{(co)j}^1 + P_{(cross)j}^1 + \|\mathbf{n}_F[\beta]\|^2}. \end{aligned} \quad (71)$$

Accordingly, in form of matrix-vector notation, the OP₁ can be formulated as follows

$$\begin{aligned} \text{OP}_{1-1}: \min_{\mathbf{p}^1} \quad & \hat{\boldsymbol{\eta}}^T \mathbf{p}^1 \\ \text{s.t.} \quad & \mathbf{p}^1 \succeq \mathbf{D}\mathbf{B}\mathbf{p}^1 + \mathbf{z}, \end{aligned} \quad (72)$$

in which, the structures of \mathbf{D} , \mathbf{B} , and \mathbf{z} are defined in Lemma 1.

Considering the objective function of OP₁₋₁, it is a fact that

$$\hat{\boldsymbol{\eta}}^T \mathbf{p}^1 = \|\hat{\boldsymbol{\eta}}\| \text{Tr}(\text{diag}(\boldsymbol{\eta})\mathbf{p}^1), \quad (73)$$

where $\boldsymbol{\eta}$ is the normalized form of $\hat{\boldsymbol{\eta}}$ which can be computed as $\boldsymbol{\eta} = \frac{\hat{\boldsymbol{\eta}}}{\|\hat{\boldsymbol{\eta}}\|}$.

On this basis, we aim at deriving the constraint of OP₁₋₁ as a function of $(\text{diag}(\boldsymbol{\eta})\mathbf{p}^1)$. After some manipulations, the constraint can be shown in a new equivalent formulation as

$$\begin{aligned} \mathbf{p}^1 \succeq \mathbf{D}\mathbf{B}\mathbf{p}^1 + \mathbf{z} \\ \Leftrightarrow \text{diag}(\boldsymbol{\eta})\mathbf{p}^1 \succeq \text{diag}(\boldsymbol{\eta})\mathbf{D}(\mathbf{B} \circ (\boldsymbol{\eta}^{-1} \mathbf{1}_{N_1 \times 1}^T)) \text{diag}(\boldsymbol{\eta})\mathbf{p}^1 + \mathbf{z}. \end{aligned} \quad (74)$$

Hence, the OP₁₋₁ can be re-formulated as

$$\begin{aligned} \text{OP}_{1-2}: \min_{\mathbf{p}^1} \quad & \|\hat{\boldsymbol{\eta}}\| \text{Tr}(\text{diag}(\boldsymbol{\eta})\mathbf{p}^1) \\ \text{s.t.} \quad & \text{diag}(\boldsymbol{\eta})\mathbf{p}^1 \succeq \text{diag}(\boldsymbol{\eta})\mathbf{D}(\mathbf{B} \circ (\boldsymbol{\eta}^{-1} \mathbf{1}_{N_1 \times 1}^T)) \\ & \quad \times \text{diag}(\boldsymbol{\eta})\mathbf{p}^1 + \mathbf{z}. \end{aligned} \quad (75)$$

Therefore, the closed-form expression of \mathbf{p}^{*1} can be given by

$$\mathbf{p}^{*1} = \text{diag}(\boldsymbol{\eta})^{-1} [\mathbf{I}_{N_1} - \text{diag}(\boldsymbol{\eta})\mathbf{D}(\mathbf{B} \circ (\boldsymbol{\eta}^{-1} \mathbf{1}_{N_1 \times 1}^T))]^{-1} \mathbf{z}. \quad (76)$$

Relying on Perron-Frobenius theory, the optimal value \mathbf{p}^{*1} is guaranteed to be a nonnegative vector if and only if the spectral radius of $\text{diag}(\boldsymbol{\eta})\mathbf{D}(\mathbf{B} \circ (\boldsymbol{\eta}^{-1} \mathbf{1}_{N_1 \times 1}^T))$ is less than unity.

Furthermore, in a special case where $\eta_1 = \eta_2 = \dots = \eta_{N_1} = \eta$, the above problem can be written in a simplified form as

$$\begin{aligned} \text{OP}_{1-3}: \min_{\mathbf{p}^1} \quad & \eta \mathbf{I}_{N_1}^T \mathbf{p}^1 \\ \text{s.t.} \quad & \mathbf{p}^1 \succeq \mathbf{D}\mathbf{B}\mathbf{p}^1 + \mathbf{z}. \end{aligned} \quad (77)$$

Then, the optimal solution of OP₁₋₂ can be given as

$$\mathbf{p}^{*1} = (\mathbf{I} - \mathbf{D}\mathbf{B})^{-1} \mathbf{z}. \quad (78)$$

One can see that the result of (78) is in agreement with that of the work in [28]. In final, the proof is completed.

APPENDIX B
PROOF OF LEMMA 2

According to (58), we can write down that

$$\begin{aligned} & \min_{\mathbf{e}_{ij}^1 \in \mathcal{F}_{ij}^1} \left| \sum_{i=1}^{M_1} (\hat{\mathbf{g}}_{ij} * \mathbf{h}_{ij}^1)[L] \right|^2 \\ &= \min_{\mathbf{e}_{ij}^1 \in \mathcal{F}_{ij}^1} \frac{\left| \sum_{i=1}^{M_1} \left(\|\mathbf{h}_{ij}^1\|^2 + (\mathbf{e}_{ij}^1)^H \mathbf{h}_{ij}^1 \right) \right|^2}{\sum_{i=1}^{M_1} \|\hat{\mathbf{h}}_{ij}^1\|^2} \\ &\stackrel{(a)}{=} \frac{\left| \sum_{i=1}^{M_1} \left(\|\mathbf{e}_{ij}^1\|^2 \left(\frac{1 - \sqrt{\psi}}{\psi} \right) \right) \right|^2}{\sum_{i=1}^{M_1} \|\hat{\mathbf{h}}_{ij}^1\|^2}. \end{aligned} \quad (79)$$

The equality in (a) is due to the fact that the quantity of $\left(\|\mathbf{h}_{ij}^1\|^2 + (\mathbf{e}_{ij}^1)^H \mathbf{h}_{ij}^1 \right)$ reaches the minimum if and only if $\mathbf{e}_{ij}^1 = -\sqrt{\psi} \mathbf{h}_{ij}^1$.

Next, by substituting $\mathbf{e}_{ij}^1 = -\sqrt{\psi} \mathbf{h}_{ij}^1$ to (59), we can obtain the following derivation

$$\|\mathbf{e}_{ij}^1\|^2 = \frac{\psi}{(1 - \sqrt{\psi})^2} \|\hat{\mathbf{h}}_{ij}^1\|^2. \quad (80)$$

Thus, we infer that

$$\min_{\mathbf{e}_{ij}^1 \in \mathcal{F}_{ij}^1} \left| \sum_{i=1}^{M_1} (\hat{\mathbf{g}}_{ij} * \mathbf{h}_{ij}^1)[L] \right|^2 = \frac{\sum_{i=1}^{M_1} \|\hat{\mathbf{h}}_{ij}^1\|^2}{(1 - \sqrt{\psi})^2}. \quad (81)$$

On the other hand, the estimated signal power can be given as

$$\left| \sum_{i=1}^{M_1} (\hat{\mathbf{g}}_{ij} * \hat{\mathbf{h}}_{ij}^1)[L] \right|^2 = \sum_{i=1}^{M_1} \|\hat{\mathbf{h}}_{ij}^1\|^2. \quad (82)$$

Accordingly, the worst-case lower-bound of signal power component can be constituted as

$$\mathcal{P}l_{(sig)_j}^1 = \left| \sum_{i=1}^{M_1} (\hat{\mathbf{g}}_{ij} * \hat{\mathbf{h}}_{ij}^1)[L] \right|^2 \frac{p_j^1}{(1 - \sqrt{\psi})^2}. \quad (83)$$

This completes the proof of Lemma 2.

APPENDIX C
PROOF OF LEMMA 3

We consider the worst-case upper-bound of $\|\hat{\mathbf{g}}_{ij} * \mathbf{h}_{ij}^1\|^2$ for simplicity. To investigate a tighter upper-bound than the value suggested in [25], [31], we introduce a novel approach in which we start with letting $\tilde{\mathbf{h}}_{ij}^1$ be a virtual channel, and we aim at investigating the optimal value $\tilde{\mathbf{h}}_{ij}^{*1}$ that makes $\|\hat{\mathbf{g}}_{ij} * \tilde{\mathbf{h}}_{ij}^1\|^2$ achieve maximal quantity. Accordingly, the problem becomes

$$\begin{aligned} & \max_{\tilde{\mathbf{h}}_{ij}^1} \quad \|\hat{\mathbf{g}}_{ij} * \tilde{\mathbf{h}}_{ij}^1\|^2 \\ & \text{s.t.} \quad \|\tilde{\mathbf{h}}_{ij}^1\|^2 \leq \max_{\mathbf{e}_{ij}^1 \in \mathcal{F}_{ij}^1} \|\mathbf{h}_{ij}^1\|^2. \end{aligned} \quad (84)$$

As observed, the problem (84) is hard to solve directly due to the convolution operator. Thus, we factorize (84) into two steps. In the first step, we let $\hat{\mathbf{G}}_{ij}$ to be a $(2L-1) \times L$ Toeplitz matrix form of $\hat{\mathbf{g}}_{ij}$, i.e. (65)

Additionally, we let $\Phi_{ij}^1 = \frac{\tilde{\mathbf{h}}_{ij}^1}{\sqrt{\max_{\mathbf{e}_{ij}^1 \in \mathcal{F}_{ij}^1} \|\mathbf{h}_{ij}^1\|^2}}$. Based on the representation of convolution with Toeplitz matrix form, the above problem can be equivalently re-formulated as

$$\begin{aligned} & \max_{\Phi_{ij}^1} \quad \left\| \left(\sqrt{\max_{\mathbf{e}_{ij}^1 \in \mathcal{F}_{ij}^1} \|\mathbf{h}_{ij}^1\|^2} \hat{\mathbf{G}}_{ij} \right) \Phi_{ij}^1 \right\|^2 \\ & \text{s.t.} \quad \|\Phi_{ij}^1\|^2 \leq 1. \end{aligned} \quad (85)$$

The closed-form derivation of optimal solution Φ_{ij}^{*1} can be obtained by computing the orthonormal eigenvector corresponding to the largest eigenvalue of the matrix $\left(\hat{\mathbf{G}}_{ij} (\hat{\mathbf{G}}_{ij})^H \max_{\mathbf{e}_{ij}^1 \in \mathcal{F}_{ij}^1} \|\mathbf{h}_{ij}^1\|^2 \right)$. Since the norm of Φ_{ij}^{*1} is equal to 1, to make a fair normalization, we devise that

$$\tilde{\mathbf{h}}_{ij}^{*1} = \frac{(\Phi_{ij}^{*1}) \|\hat{\mathbf{h}}_{ij}^1\|}{(1 - \sqrt{\psi})}, \quad (86)$$

where $\tilde{\mathbf{h}}_{ij}^{*1}$ is the optimal value regarding to the achievement the maximum of $\|\hat{\mathbf{g}}_{ij} * \tilde{\mathbf{h}}_{ij}^1\|^2$, and $\max_{\mathbf{e}_{ij}^1 \in \mathcal{F}_{ij}^1} \|\mathbf{h}_{ij}^1\|^2 = \frac{\|\hat{\mathbf{h}}_{ij}^1\|^2}{(1 - \sqrt{\psi})^2}$.

Therefore, we can obtain a new boundary from (86) as

$$\begin{aligned} & \max_{\mathbf{e}_{ij}^1 \in \mathcal{F}_{ij}^1} \left\| \sum_{i=1}^{M_1} \hat{\mathbf{g}}_{ij} * \mathbf{h}_{ij}^1 \right\|^2 \\ &= \sum_{i=1}^{M_1} \|\hat{\mathbf{g}}_{ij} * \tilde{\mathbf{h}}_{ij}^{*1}\|^2 + \left\| \sum_{i=1}^{M_1} \sum_{i' \neq i}^{M_1} (\hat{\mathbf{g}}_{ij} * \tilde{\mathbf{h}}_{ij}^{*1})^H (\hat{\mathbf{g}}_{i'j} * \tilde{\mathbf{h}}_{i'j}^{*1}) \right\|. \end{aligned} \quad (87)$$

Thus, the proof of Lemma 3 is completed.

REFERENCES

- [1] T. Zahir, K. Arshad, A. Nakata, and K. Moessner, "Interference management in femtocells," *IEEE Comm. Surveys & Tutorials*, vol. 15, no. 1, pp. 293–311, 2013.
- [2] E. Hossain and M. Hasan, "5g cellular: Key enabling technologies and research challenges," *IEEE Instrum. Meas. Mag.*, vol. 18, no. 3, pp. 11–21, June 2015.
- [3] S. Buzzi, C.-L. I, T. E. Klein, H. V. Poor, C. Yang, and A. Zappone, "Energy-efficient techniques for 5g networks and challenges ahead," *IEEE J. Sel. Areas Commun.*, vol. 34, no. 4, pp. 697–709, April 2016.
- [4] J. Andrews, H. Claussen, M. Dohler, S. Rangan, and M. Reed, "Femto-cells: Past, present, and future," *IEEE J. Sel. Areas Commun.*, vol. 30, no. 3, pp. 497–508, 2012.
- [5] M. Bennis, L. Giupponi, E. Diaz, M. Lalam, M. Maqbool, E. Strinati, A. De Domenico, and M. Latva-aho, "Interference management in self-organized femtocell networks: The befemto approach," in *Proc. of 2nd International Conference on Wireless Communication, Vehicular Technology, Information Theory and Aerospace & Electronic Systems Technology (Wireless VITAE)*, 2011, pp. 1–6.

- [6] V. Tran-Ha, Q.-D. Vu, and E.-K. Hong, "Time reversal-based transmissions with distributed power allocation for two-tier networks," in *Proc. of IEEE 29th International Conference on Advanced Information Networking and Applications Workshops (WAINA)*, 2015, pp. 181–186.
- [7] T. Kaiser and F. Zheng, *Ultra-wideband Systems with MIMO*. Wiley, 2010.
- [8] M.-A. Bouzigues, I. Siaud, M. Helard, and A.-M. Ulmer-Moll, "Turn back the clock: Time reversal for green radio communications," *IEEE Veh. Technol. Mag.*, vol. 8, no. 1, pp. 49–56, 2013.
- [9] M. Maaz, M. Helard, P. Mary, and M. Liu, "Performance analysis of time-reversal based precoding schemes in miso-ofdm systems," in *Proc. IEEE 81st Vehicular Technology Conference (VTC Spring)*, May 2015, pp. 1–6.
- [10] Y. Chen, B. Wang, Y. Han, H.-Q. Lai, Z. Safar, and K. R. Liu, "Why time reversal for future 5g wireless? [perspectives]," *IEEE Signal Processing Magazine*, vol. 33, no. 2, pp. 17–26, 2016.
- [11] A. Pitarokoulis, S. Mohammed, and E. Larsson, "Uplink performance of time-reversal MRC in massive MIMO systems subject to phase noise," *IEEE Trans. Wireless Commun.*, vol. 14, no. 2, pp. 711–723, 2015.
- [12] I. Siaud, A.-M. Ulmer-Moll, M.-A. Bouzigues, and N. Cassiau, "Adaptive and spatial processing for millimeter wave backhaul architectures," in *Proc. IEEE International Conference on Ubiquitous Wireless Broadband (ICUWB)*, 4-7 Oct 2015.
- [13] C. A. Viteri-Mera, F. L. Teixeira, and K. Sainath, "Interference-nulling time-reversal beamforming for mm-wave massive mimo systems," in *Proc. IEEE Int. Conf. Microw., Commun., Antennas Electron. Syst. (COMCAS)*, 2015, pp. 1–5.
- [14] C. A. Viteri-Mera and F. L. Teixeira, "Space-time block diagonalization for frequency-selective mimo broadcast channels," *IEEE Access*, vol. 4, pp. 6602–6613, 2016.
- [15] Y.-H. Yang, B. Wang, W. Lin, and K. Liu, "Near-optimal waveform design for sum rate optimization in time-reversal multiuser downlink systems," *IEEE Trans. Wireless Commun.*, vol. 12, no. 1, pp. 346–357, 2013.
- [16] E. Yoon, S.-Y. Kim, and U. Yun, "A time-reversal-based transmission using predistortion for intersymbol interference alignment," *IEEE Trans. Commun.*, vol. 63, no. 2, pp. 455–465, February 2015.
- [17] B. E. Henty and D. D. Stancil, "Multipath-enabled super-resolution for rf and microwave communication using phase-conjugate arrays," *Physical Review Letters*, vol. 93, no. 24, p. 243904, 2004.
- [18] H. T. Nguyen, J. Pedersen, P. Kyritsi, and P. Eggers, "Time reversal in wireless communications: a measurement based investigation," *IEEE Trans. Wireless Commun.*, vol. 5, no. 8, pp. 2242–2252, 2006.
- [19] A. Tolli, H. Pennanen, and P. Komulainen, "Decentralized minimum power multi-cell beamforming with limited backhaul signaling," *IEEE Trans. Wireless Commun.*, vol. 10, no. 2, pp. 570–580, 2011.
- [20] A. Rozé, M. H  lard, M. Cruss  re, and C. Langlais, "Linear precoder performance for massive mimo systems in near los environments: Application to mmwave transmission," in *Proc. of 21th European Wireless Conference*. VDE, 2015, pp. 1–6.
- [21] Q.-D. Vu, L.-N. Tran, R. Farrell, and E.-K. Hong, "Energy-efficient zero-forcing precoding design for small-cell networks," *IEEE Trans. Commun.*, vol. 64, no. 2, pp. 790 – 804, Feb. 2016.
- [22] C. Peel, B. Hochwald, and A. Swindlehurst, "A vector-perturbation technique for near-capacity multiantenna multiuser communication-part i: channel inversion and regularization," *IEEE Trans. Commun.*, vol. 53, no. 1, pp. 195–202, 2005.
- [23] Y. Joeng, T. Q. Quek, and H. Shin, "Beamforming optimization for multiuser two-tier networks," *Journal of Communications and Networks*, vol. 13, no. 4, August 2011.
- [24] D. Nguyen, L. B. Le, and T. Le-Ngoc, "Multiuser admission control and beamforming optimization algorithms for miso heterogeneous networks," *IEEE Access*, vol. 3, pp. 759–773, 2015.
- [25] W. H. Young, "On the multiplication of successions of fourier constants," *Proc. Roy. Soc. Lond. Series A*, vol. 87, pp. 331–339, 1912.
- [26] M. Trott, *The Mathematica guidebook for symbolics*. Springer Science & Business Media, 2007.
- [27] M. Bengtsson and B. Ottersten, *Optimal and Suboptimal Transmit Beamforming*. CRC Press, 2001.
- [28] V. Chandrasekhar, J. G. Andrews, T. Muharemovic, Z. Chen, and A. Gatherer, "Power control in two-tier femtocell networks," *IEEE Trans. Wireless Commun.*, vol. 8, no. 8, pp. 4316–4328, 2009.
- [29] M. Grant and S. Boyd, *CVX: Matlab software for disciplined convex programming*, June 2009.
- [30] Bogachev and V. I., *Measure Theory I*. New York: Springer-Verlag, 2007.
- [31] W. Beckner, "Inequalities in fourier analysis," *Ann. of Math.*, vol. 102, no. 1, pp. 159–182, 1975.
- [32] S. Bobkov, M. Madiman, and L. Wang, "Fractional generalizations of young and brunn-minkowski inequalities," *Contemporary Mathematics*, vol. 545, 2011.
- [33] M. Hernandez, H.-B. Li, I. Dotlic, and R. Miura, "Channel models for TG8," IEEE, Tech. Rep., 2012. [Online]. Available: <https://mentor.ieee.org/802.15/dcn/12/15-12-0459-06-0008-tg8-channel-models.doc>